



Review

Understanding the Links between LULC Changes and SUHI in Cities: Insights from Two-Decadal Studies (2001–2020)

Ahmed Derdouri ¹, Ruci Wang ^{2,*}, Yuji Murayama ² and Toshihiro Osaragi ¹

¹ School of Environment and Society, Tokyo Institute of Technology, 2 Chome-12-1 Ookayama, Meguro City, Tokyo 152-8550, Japan; derdouri.a.aa@m.titech.ac.jp (A.D.); osaragi.t.aa@m.titech.ac.jp (T.O.)

² Faculty of Life and Environmental Sciences, University of Tsukuba, 1-1-1 Tennodai, Tsukuba City 305-8572, Ibaraki, Japan; mura@geoenv.tsukuba.ac.jp

* Correspondence: wang.ruci.fw@u.tsukuba.ac.jp

Abstract: An urban heat island (UHI) is a serious phenomenon associated with built environments and presents threats to human health. It is projected that UHI intensity will rise to record levels in the following decades due to rapid urban expansion, as two-thirds of the world population is expected to live in urban areas by 2050. Nevertheless, the last two decades have seen a considerable increase in the number of studies on surface UHI (SUHI)—a form of UHI quantified based on land surface temperature (LST) derived from satellite imagery—and its relationship with the land use/cover (LULC) changes. This surge has been facilitated by the availability of freely accessible five-decade archived remotely sensed data, the use of state-of-art analysis methods, and advancements in computing capabilities. The authors of this systematic review aimed to summarize, compare, and critically analyze multiple case studies—carried out from 2001 to 2020—in terms of various aspects: study area characteristics, data sources, methods for LULC classification and SUHI quantification, mechanisms of interaction coupled with linking techniques between SUHI intensity with LULC spatial and temporal changes, and proposed alleviation actions. The review could support decision-makers and pave the way for scholars to conduct future research, especially in vulnerable cities that have not been well studied.

Keywords: urban heat island (UHI); land use land cover (LULC); land surface temperature (LST); spatiotemporal changes; SUHI-contributing factors; satellite imagery; literature review



Citation: Derdouri, A.; Wang, R.; Murayama, Y.; Osaragi, T. Understanding the Links between LULC Changes and SUHI in Cities: Insights from Two-Decadal Studies (2001–2020). *Remote Sens.* **2021**, *13*, 3654. <https://doi.org/10.3390/rs13183654>

Academic Editor: Zina Mitraka

Received: 11 August 2021

Accepted: 10 September 2021

Published: 13 September 2021

Publisher's Note: MDPI stays neutral with regard to jurisdictional claims in published maps and institutional affiliations.



Copyright: © 2021 by the authors. Licensee MDPI, Basel, Switzerland. This article is an open access article distributed under the terms and conditions of the Creative Commons Attribution (CC BY) license (<https://creativecommons.org/licenses/by/4.0/>).

1. Introduction

Since the start of the industrial revolution in Great Britain circa the 1780s [1], substantial urban expansion and population growth have been observed in industrialized countries. To put things in perspective, there were fewer than 50 cities with over 100,000 residents in 1800, there were approximately 900 cities in 1950 [2], and there were thousands of cities in 2019 [3]. In fact, by the end of the last century, almost 370 cities had over one million inhabitants worldwide, which increased to 584 in 2018, and it is estimated to reach 706 cities by the end of 2030 [4]. Though these accelerated trends have contributed to economic growth and social development in many parts of the world, they have also led to several environmental issues at different scales. Urban heat islands (UHIs) are perhaps the most evident and most documented manifestation of these radical anthropogenic activities.

UHI, also known as an “urban heat sink” or an “oasis effect” [5], refers to the phenomenon that occurs in urban areas (UAs) that involves an excessive increase in interrelated air, subsurface, and surface temperatures compared to those observed in underdeveloped surroundings [6]. The common term “heat island”—reportedly coined by British climatologist Gordon Manley in 1958 [7]—was given its name because the resulting spatial shape of the isotherms creates one or more island-like features [8]. The UHI phenomenon was first documented by Luke Howard over 200 years ago in his study of London’s climate, where he found fluctuations in temperatures measured in the city and its rural surroundings

during daytimes and nighttimes—the city had 3.7 °F warmer nights and 0.34 °F colder days than the countryside [9]. Statistically, UHIs have been documented in over 1400 cities across the globe in all continents without exception [10].

Urbanization has been highlighted in numerous studies as the leading culprit behind UHIs. Economic growth usually drives new UAs to accommodate new industrial and commercial hubs and ultimately build connecting transportation networks and new residences, especially for a floating population hoping for stable life away from numerous hardships and the lack of opportunities associated with rural areas. Perhaps, urbanization leads to social stability and economic prosperity; on the other hand, land cover conversion to urban uses has detrimental effects on the balance of the natural environment. Natural surfaces, including vegetation and water bodies, contribute to the balance of energy heat fluxes because they are excellent solar radiation absorbers. Vegetation uses a significant amount of the absorbed radiation through evapotranspiration to release water vapor that subsequently helps to cool the air in their proximity [11].

Additionally, vegetation reduces surface temperatures by offering a shading layer that shields land surfaces from direct sun radiation [12]. Water bodies provide cooling effects, much as vegetation does, as they provide a source for moisture capable of lowering nearby ambient temperatures. By contrast, impervious surfaces (ISs) such as concrete (buildings) and asphalt (streets) halt the interchange of heat between different environmental components because of their low reflectivity and capacity to absorb solar radiation [13], leading to heat imbalance and, consequently, local climate change. Ultimately, the alteration of previous surfaces to ISs introduces perturbations into the balance of the local climate, resulting in UHIs. Moreover, the heat emitted by traffic, industries, factories, and air conditioners contributes to increasing the local temperature [14]. Additionally, the amount of airflow is reduced as narrow streets and tall buildings trap heat, thereby intensifying the heat island effect [14].

In the short and long term, UHIs have severe implications for many areas of life on earth, including socioeconomic and environmental issues. Air pollution may increase because of UHIs, daytime temperatures become warmer, and nighttime cooling becomes less effective [15]. These alterations lead to discomfort and an increase in human premature mortality rates due to excessive heat. In fact, extreme heat is a primary contributor to the rise in weather-related human mortality [16–18]. Between 1991 and 2018, 37% of the world's heat-related fatalities may have been linked to human-caused global warming [19]. Additionally, because of UHIs, urban rain islands can form, resulting in greater precipitation during the flood season in flood-prone places and leading to waterlogging at a regional scale [20]. In Jinan City, for instance, it has been proven that the URI effect is spatially correlated with that of the UHI, resulting in an increased frequency and severity of short-duration precipitation episodes [21]. During the rainy season, areas with intensive construction receive more rain. With so much rain concentrated in urbanized areas, which are characterized by low surface infiltration capacities, the city has become more and more vulnerable to floods.

The UHI phenomenon is also an obstacle to achieving sustainable development. In 2015, the United Nations provided the 17 Sustainable Development Goals (SDGs), four of which are directly or indirectly related to UHIs. UHIs comprise one of the significant reasons for apparent temperature increases, which have the potential to be particularly serious for heat-associated deaths (SDG 3 (Good Health and Well-Being)), and people who are living in high-temperature areas also have increased electricity bills (SDG 7 (Affordable and Clean Energy)). Additionally, high-rise and -density buildings lead to UHIs and can affect the quality of eco-environments in living areas (SDG 11 (Sustainable Cities and Communities)). UHIs can also influence urban microclimates, and in the long run, their effects could indicate global warming (SDG 13 (Climate Action)). According to the United Nations, 60% of the world's people (around 5 billion) will live in UAs by 2050. The increase in urban populations will be the cause of urban agglomeration, and then UHIs will become more obvious. Therefore, the proper awareness and analysis of the relationship between

UHIs and land use land cover (LULC) changes, as well as how to relieve the UHI effect by urban planning, are crucial for achieving the SDGs.

Broadly, UHIs can be categorized into two types: surface UHIs (SUHIs) and atmospheric UHIs (AUHIs). Several aspects differentiate the two UHI forms, as summarized by Sharma and Joshi [22]: (i) day/night prominence: during daytimes and nighttimes, SUHIs are prominent, while AUHIs are mainly noticeable at night [23]; (ii) seasonal variations: during wintertime, AUHIs are more intense than SUHIs and vice versa in the summertime [24,25]; (iii) UHI intensity (UHII): SUHI intensity generally tends to be much higher than AUHI intensity [26]; (iv) data sources: while AUHI measurements are mostly retrieved from ground-based meteorological stations network and field surveys, SUHI measurements are quantified using airborne or satellites thermal data [27,28]; and (v) ideal observation time: nighttimes under a clear sky and calm conditions are the best times for investigating AUHIs, but thermal data taken during the daytimes are more suitable for investigating SUHIs [29].

Furthermore, Oke distinguished two types of AUHIs [30]: the urban canopy layer (UCL) and the urban boundary layer (UBL). A UCL is formed by microscale activities occurring in urban streets—often referred to as “canyons”—that connect buildings situated under the roofline [31]. By contrast, a UBL is a localized mesoscale phenomenon that is influenced by the nature of the urban topography above the roofline [31]. Fixed and mobile instruments can be used to observe UBLs and UCLs. While the most common devices used to monitor UCLs are fixed screens and automobiles, UBLs can be observed using fixed tower sodars or aircrafts and tetroons [32]. However, these instruments and techniques are time- and budget-consuming, especially when focusing on city-, metropolitan-, or mega-city-scale and regional studies. Moreover, the availability of historical or up-to-date measurements is another obstacle that hinders investigating historical trends of AUHIs. Conversely, using satellite-derived data, spatiotemporal studies of SUHI distribution may be conducted in a cost-effective and time-saving manner [33] at local and regional scales.

The use of remotely sensed data to study urban climate started in the 1970s as a result of successful observational satellite programs such as Television InfraRed Observational Satellite (TIROS), Nimbus, Environmental Science Services Administration Satellite (ESSA), and Landsat, resulting in the launch of several satellites—notably TIROS-1 (1960), Nimbus series (1964–1978), ESSA-1 (1966), and Landsat series (since 1972). Reportedly, Rao may have been the first to show that satellite imagery can be used to investigate urban climate [34]. Through his study, he investigated surface temperature trends in cities across the Mid-Atlantic coast of the US using the infrared radiometer (IR) data of TIROS-I. Subsequently, other studies using similar approaches followed. For instance, Matson et al. used NOAA-5 satellite data to identify nocturnal UHIs in the Midwest and Northwestern US [35], and Price investigated UHIs in New York City and the New England region [36]. Taking advantage of the significant advancements in computing software and hardware in the last two decades, researchers have been able to concisely investigate SUHIs and their driving factors vis-à-vis LULC in different regions of the world, relying on sophisticated developed techniques to retrieve land surface temperatures (LSTs) and extract LULC information from freely accessible historical satellite data covering almost half a century of data. Particularly, Landsat series data have been extensively used to evaluate the connection between LULC and LST.

Several review studies have been published in recent years that summarize our knowledge on SUHIs from multiple perspectives, including LST retrieval methods from thermal sensors [37], exploring factors amplifying its intensity [38], and mitigation strategies [39]. Deilami et al., for instance, focused on how spatial factors (e.g., LULC and urban form), dynamics, and temporal variations (e.g., yearly and seasonal) impact SUHIs. The authors reviewed studies published between 1965 and 2017 [38]. In a broad yet comprehensive review, Zhou et al. explored several aspects based on the literature published from 1972 to 2018 [10]. The authors investigated the popular thermal sensors and methods used to retrieve SUHIs from them in addition to the main drivers of SUHI variations. While most

review studies have focused on a worldwide geographic scope, others have focused on a concise geographic scale limited to a region or even a country. Kotharkar et al., for instance, concentrated their review on South Asian cities because the region hosts approximately 15% of the world's population [40]. The authors reviewed published papers between 1973 and 2017, with a primary focus on investigating empirical measurements of UHIs, observation, modeling, their impact, and proposed mitigation strategies.

In this review paper, however, we focus on how spatial and temporal changes of different factors, in particular those related to LULC, have impacted SUHIs in cities across the globe from the turn of the 21st century till the present. In addition to the characteristics of the reviewed literature in terms of annual trends, sources, and geographical coverage, a detailed key points analysis that concerns five critical topics was conducted: (1) the primary data sources and methods employed for extracting LULC and retrieving LST information, (2) the methods used for evaluating LULC and SUHIs, (3) the most common factors deemed critical in affecting SUHI magnitude across time and space, (4) an overview of the proposed mitigation strategies, and finally (5), the main limitations and future directions.

With that in mind, the overall structure of this review takes the form of five sections, excluding this introductory section. Section 2 is concerned with the followed review methodology, specifically the selection criteria of the reviewed literature and the main considered databases. Section 3 presents a general synopsis of the findings of the review, focusing on the synthesis of the literature and geographical coverage of the reviewed studies. In Section 4, a detailed analysis of the obtained results focusing on seven key elements is presented: (i) the main satellite data sources, (ii) the methods of LULC extraction, (iii) the methods of SUHI quantification, (iv) the assessment methods of the relationship between LULC and SUHIs, (v) the main factors affecting UHIs, (vi) the proposed mitigation strategies, and lastly (vii), the future challenges and areas for further research. Section 5 summarizes the findings.

2. Review Methodology

In this review, we concentrated on the literature focusing on connections between LULC spatiotemporal changes and UHIs, specifically SUHIs extracted from satellite images. For that reason and because satellite images have become more accessible, we concentrated on studies published in the last two decades—precisely between January 2001 and November 2020. The management of remotely sensed data has become easy, thanks to the advancement of GIS in terms of software and hardware (computer performance). Three databases were explored, namely: Scopus, Web of Science, and Google Scholar. Furthermore, only peer-reviewed journal articles written in English were retained. Conference papers, book chapters, reports, and other types were excluded.

Regarding the followed inclusion strategy, we employed a four-step approach (Figure 1) to screen the existing literature. First, we identified published papers based on a broad search query. Considering the varying terminology employed by researchers, we built search queries by combining possible variants of key terms including: “UHI”, “urban heat island”, “land use”, “LULC”, “spatiotemporal”, and “satellite image”. Second, we conducted an initial assessment of the resulting papers based on their titles and abstracts. We excluded unrelated papers, including health- and energy-focused and climatology-related papers—notably those concerning simulation and numeric modeling. Third, a deeper screening was conducted to further refine the resulting papers from the previous screening based on the content of each paper, following the filtering out of duplicated papers collected from the three considered indexing databases. Through this deep screening, we ensured that the included manuscripts satisfied the following requirements:

- At least two-date satellite images were used to analyze changes of LULC and SUHIs.
- The authors explicitly assessed the relationship between the different LULC classes and SUHIs.
- The study was city-focused; district-level and regional-level studies were excluded.
- For multicity studies, we considered each city as a case study.

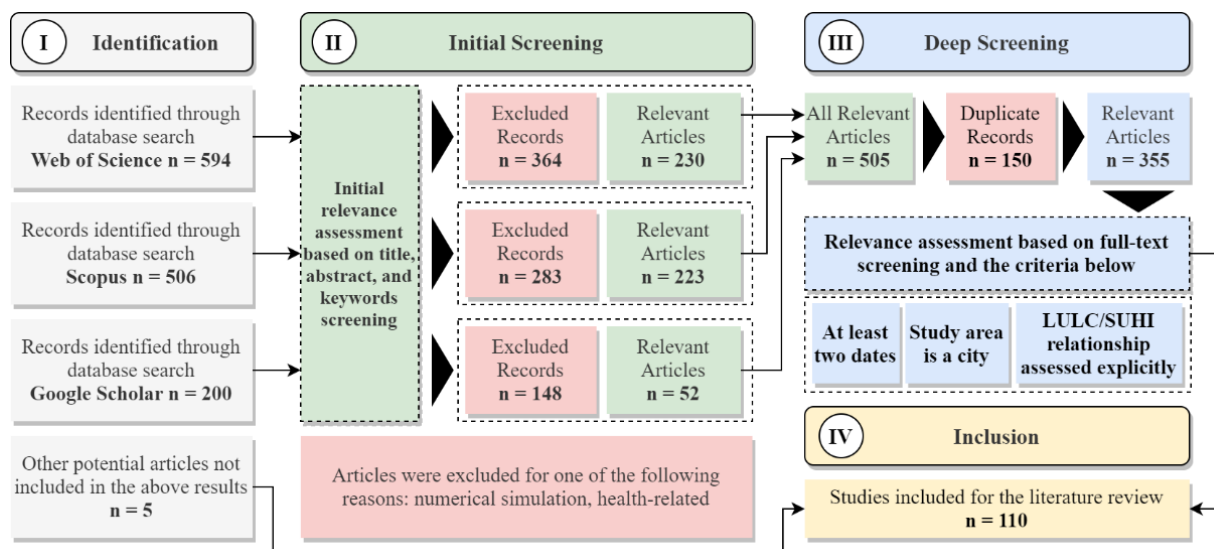


Figure 1. Methodological flowchart.

This process yielded a total of 110 eligible papers out of 1300 (duplicates included) initially found, based on selection queries. Three other studies that fit our inclusion criteria were added because they were not included in the query-based search results. Relevant attributes for each retained manuscript—including author(s), title, source, year of publication, and keywords—were collected. Additionally, we gathered the characteristics of the target area(s), namely: country, climate region, type (i.e., landlocked or coastal), and size (via population and/or spatial extent). Information related to spatiotemporal LULC changes was also recorded. We focused on study period, data sources, considered seasons, day/night, and LULC extraction method(s). A detailed list of all included studies with a brief description of used methods, the characteristics of the study area(s), and results is presented in the Supplementary Materials.

3. General Findings

This section presents a descriptive statistical analysis of the gathered literature. Section 3.1 describes the statistical results regarding the yearly growth and publication sources of the selected papers. Section 3.2 provides insights regarding the investigated cities in terms of their geographical distribution concerning their physical characteristics (e.g., climate and topography). Section 3.3 describes the general characteristics of the reviewed publications in terms of the selected study areas and study periods.

3.1. Literature Synopsis: Trends and Source

Figure 2 shows the yearly counts of published papers investigating the relationship between LULC changes and SUHIs. Two noteworthy findings emerge from these counts. First, the usage of satellite images to investigate UHIs vis-à-vis spatiotemporal LULC changes is still in its initial phase, which is reflected by the short period and a small number of annually published studies (25 at most). It should be noted that the lower number of studies was possibly due to the selection criteria we adopted, as we required at least two dates to analyze LULC changes and, subsequently, SUHIs. The reader is referred to a more inclusive review by Zhou et al. regarding a longer coverage time range and looser inclusion criteria [10]. Second, a generally increasing tendency in the annual numbers can be seen, especially since 2010, suggesting a rising interest in this research topic. This could be attributed to the fact that medium-spatial-resolution Landsat data have been made freely accessible since then. Furthermore, the significant optimization of computing capabilities (e.g., big data storage and short execution/processing timing) in the last two decades, together with the significant and constant improvement in GIS and

remote sensing methods, has attracted a growing number of researchers to contribute to this important topic.

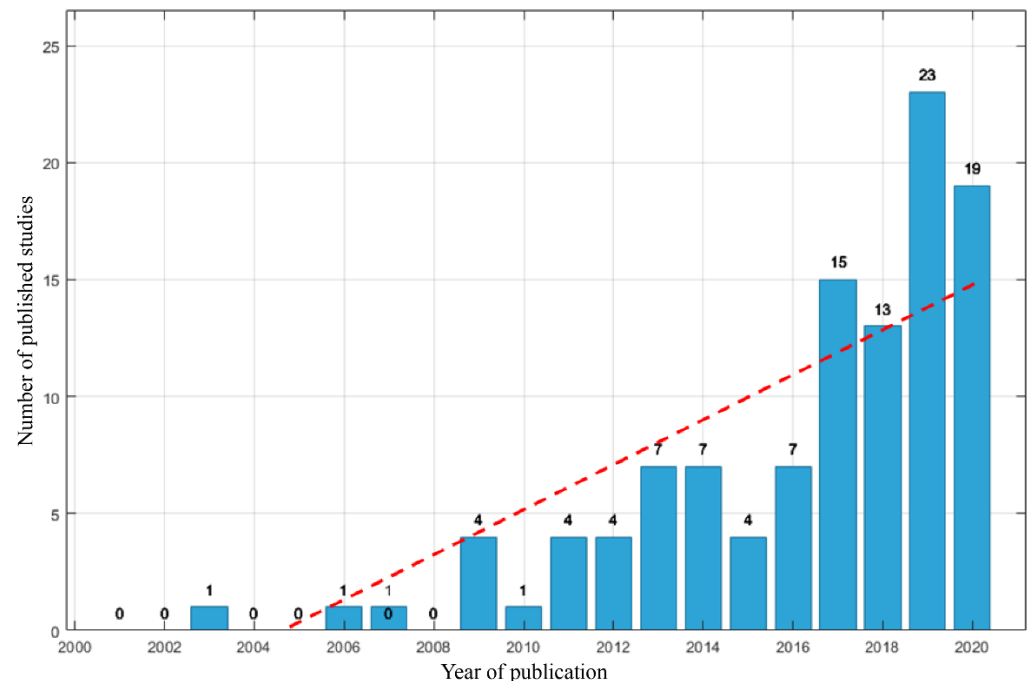


Figure 2. Annual trends of the published literature regarding studies' investigations of SUHI/LULC changes.

In terms of publication sources, the selected literature appeared in 61 journals. A vast majority of studies were published in *Sustainability* (10.8%) and *Urban Climate* (9.6%). Other top leading journals included the *International Journal of Remote Sensing*, *Remote Sensing*, and *Sustainable Cities and Society*, with 7.2% each. About 6% of articles were published in the *International Journal of Applied Earth Observation and Geoinformation* and *ISPRS Journal of Photogrammetry and Remote Sensing*.

3.2. Geographical Coverage and Cities Characteristics

Figure 3 displays the geographical distribution of the investigated studies. It should be noted that the number of studies does not correspond to the number of cities, as several considered studies analyzed multiple cities at once, notably [41], where the authors investigated the interlacement between LULC changes and the magnitude of UHIs in 10 Indian cities.

From a geographical standpoint, SUHI–LULC links investigated in 133 cities of 27 countries worldwide were reported. Figure 3 illustrates the spatial distribution of the total numbers of the considered studies in every country. Investigations focusing on Asian cities were predominant (83.2%). Few studies focused on cities in Africa (6.6%), South America (3.6%), North America (2.9%), Europe (2.2%), and Oceania (1.5%).

In terms of climatological characteristics, the spatial distribution and percentage of investigated cities based on their zones on the Köppen–Geiger climate system—according to a recent update published in [42]—are illustrated in Figure 3 and Table 1. Most investigated cities (42%) are characterized by a temperate climate. Specifically, those located in humid subtropical (Cfa) and dry-winter humid subtropical (Cwa) were found to represent 23.4% and 12.4% of all investigated cities, respectively. Most of these cities are located in Asia, such as Shanghai, Fuzhou, and Wuhan for Cfa and Guangzhou, Shenzhen, and Hanoi for Cwa. These climates are generally characterized by mild-to-warm summers and cool-to-cold winters [43]. Desert-climate cities were also found to be common target areas, as about 25% of all cities are located in such climate regions, most likely because UHIs thrive in such climates due to limited vegetation cover and water resources. Researchers have mainly

focused on cities with hot arid (BWh) and hot semiarid (BSh) climates, with each of them representing 10% of the total considered cities. Another 23% of the examined cities belong to the tropical climates, with a focus on cities enjoying Aw (tropical savanna) climate (14%). Constant high temperatures typically characterize a tropical climate. Continental-climate cities were found to be the least investigated, with a share of only 10%, and approximately 7% of these studies focused on the Dwa (hot summer continental) climate. This climate has warm months that average between 10 and 20 °C, and its cold months are at or below 0 °C.

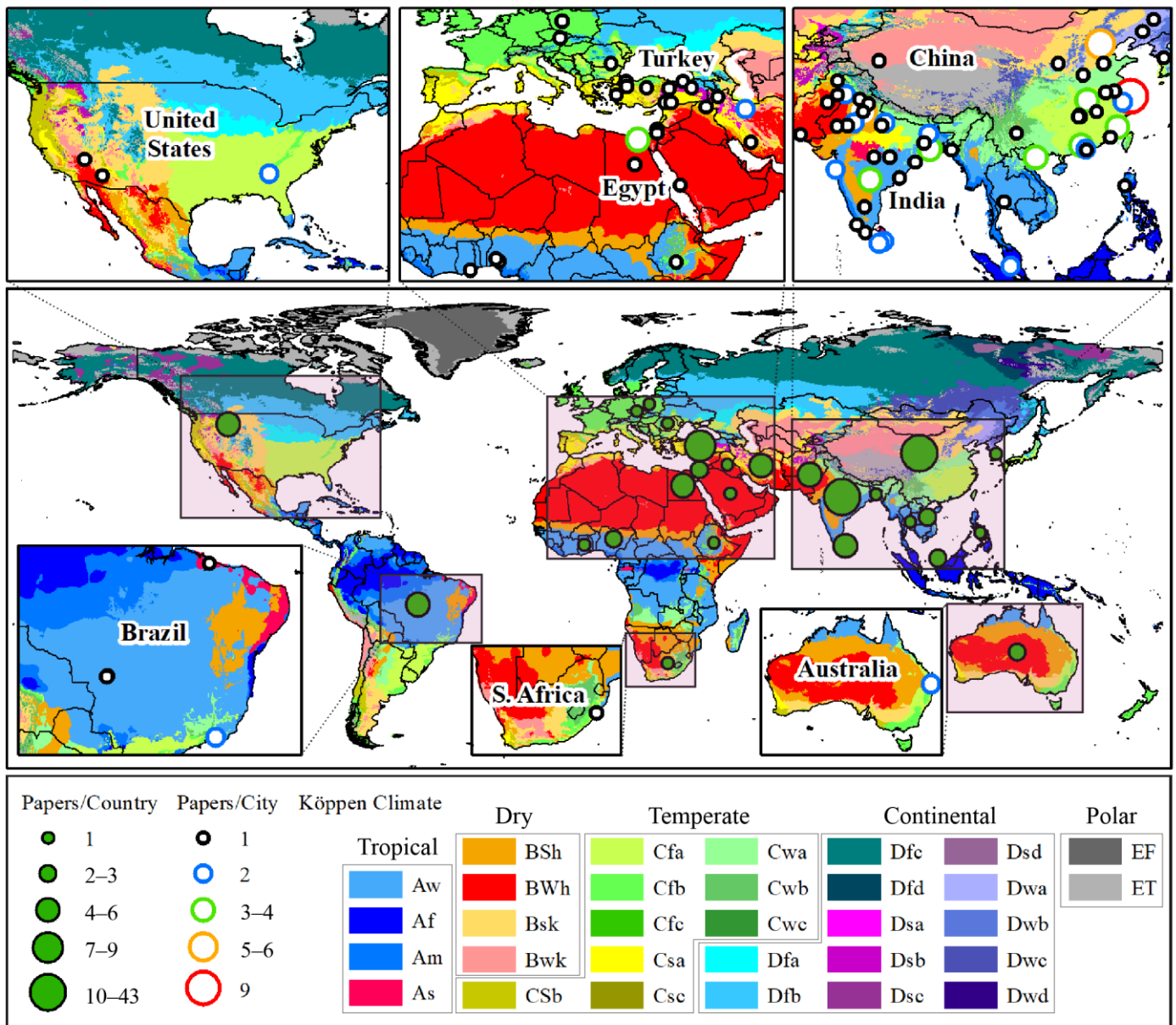


Figure 3. Spatial distribution of case studies aggregated based on countries where cities are located with regard to the world’s Köppen climate classification according to [42] (licensed under CC BY 4.0). The circle size on the left indicates the range of papers count per country.

Overall, cities with hot summers (BSh, BWh, and Dwa), and humid/dry winters (Cfa, Cwa, and Aw) were found to be the most investigated cities. The focus on cities under these specific climates is attributed to many reasons. First, increasing SUHI magnitudes directly impacts climate change and urban expansion, especially since most cities under these climate regimes are situated in developing countries. Second, in contrast to tropical and continental cities, satellite data covering desert cities are not ruined by high percentages of

clouds during most seasons of the year. This specific issue, which is discussed in detail in Section 4.7.1, is the most challenging obstacle facing studies investigating SUHIs in general and particularly those focusing on connections between SUHIs and LULC over wide areas and long time.

Table 1. Share of studies regarding the climate regions classified based on Köppen climate classification.

Temperate					Arid				Tropical			Continental	
41.6%					24.8%				23.4%			10.2%	
Cfa	Cwa	Csa	Csb	Cwb	BSh	BWh	BSk	BWk	Aw	Am	Af	Dwa	Dfa
23.4%	12.4%	4.4%	0.72%	0.72%	10.2%	10.2%	3.6%	0.7%	13.9%	5.1%	4.4%	7.3%	0.7%

3.3. General Characteristics: Study Periods and Target Areas

The use of historical remotely sensed data going back to the 1970s has made it possible to study decadal LULC spatiotemporal changes, as well as their impact on LST. Over half of the studies used research durations of more than 10 years, as shown in Figure 4. Selecting such lengthy periods helped provide distinct contrasts between past and current trends.

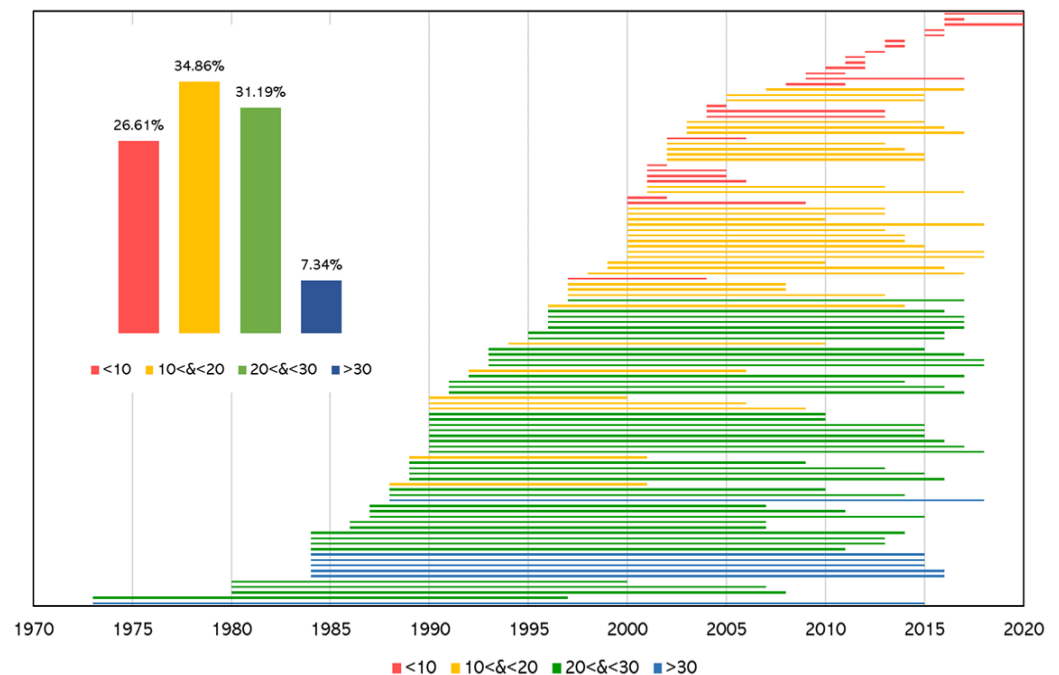


Figure 4. Timeline of study periods considered in the reviewed literature along with the percentage of studies based on different decadal time intervals.

To accommodate explosive population increases in developing countries while ensuring faster economic growth, urbanization rates in such countries are generally faster than those observed in developed countries. Previous studies have affirmed that urban expansion is one of the leading drivers of SUHI development in UAs. These facts are reflected in the number of target areas in developing countries presented in Figure 5, illustrating the number of reviewed studies per country categorized according to their development indexes [44]. In detail, compared to 7.3% in developed countries, 92.7% of investigations were reported in developing nations. Chinese and Indian cities have been the most investigated. Shanghai was ranked first, with nine publications [20,45–52], followed by Delhi [22,53–56] and Beijing [48,57–60], with five publications each.

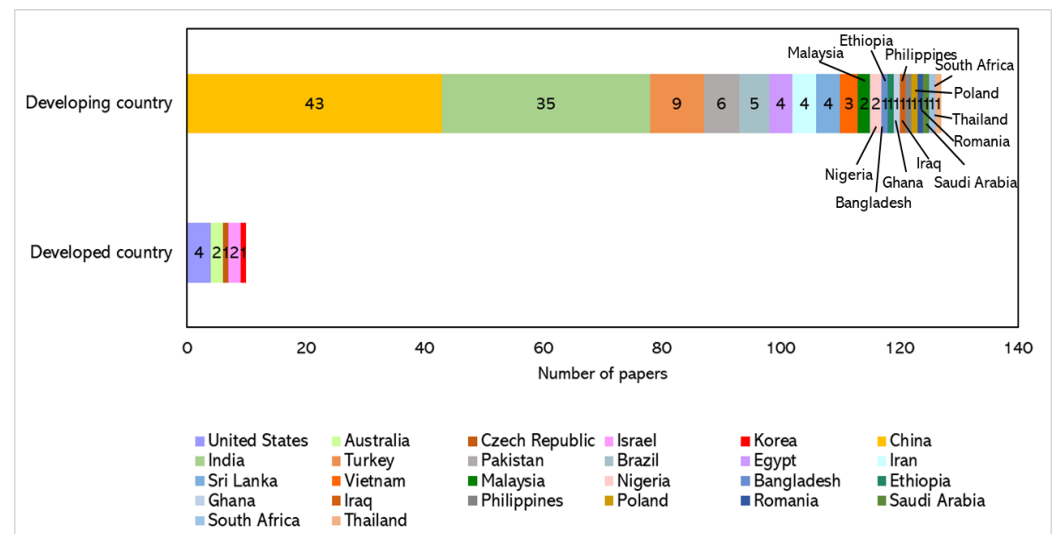


Figure 5. The number of studies that focused on cities in developed and developing nations.

4. Content Key Focuses

This section focuses on the key elements used in the literature to study the interconnections between LULC changes and SUHIs. Firstly, we identify and compare the main data sources used in terms of offered advantages and limitations (Section 4.1). Secondly, we detail the most common techniques of LULC extraction (Section 4.2) and SUHI calculation (Section 4.3). Thirdly, qualitative and quantitative methods for analyzing the association of LULC and UHI changes in cities are detailed (Section 4.4). Next, we provide an overview of the factors affecting SUHIs (Section 4.5). Finally, the mitigation strategies recommended in the considered literature (Section 4.6), followed by the limitations and future directions (Section 4.7), are summarized.

4.1. Data Sources

Table 2 shows the most common satellite data sources used to extract LULC changes and/or LST retrieval. Landsat series satellite data were found to have been dominant among researchers (95.5%), followed by MODIS (10.9%) and ASTER (4.5%). Only one study relied on HJ-1B data (0.9%). Other sources of imagery were found to include high-resolution satellites mainly used for LULC classification validation purposes such as IKONOS [61], SPOT [62,63], IRS LISS-III [64], and Sentinel 2A [65]. Additionally, Table 2 shows the percentage of studies based on the considered study periods. Landsat data are often used for all study period ranges—specifically for periods between 10 and 20 years (37%). MODIS data, on the other hand, are generally used in medium-study-period studies (50%). Regarding high-resolution imagery, they were used extensively in studies focusing on medium-period studies (43%). It should be noted that this imagery type is generally used for validation of LULC classification rather than LULC changes analysis.

Landsat series satellite data were used in approximately 95.9% of the considered literature for LULC extraction, LST retrieval, or (mostly) for both. More than half of reviewed studies (77.6%) were found to have used Landsat series data to investigate medium-to-very-long (more than 10 years) LULC changes between 1980 and 2020 (Table 2). As a cooperation program between the National Aeronautics and Space Administration (NASA) and the United States Geological Survey (USGS), the series has been operating since 1972 and consists of eight satellites that can image the earth in moderate resolution. They are considered to comprise the longest-running optical remote-sensing-based satellite constellation for monitoring the earth. The Landsat Multispectral Scanner (MSS) was used on Landsat 1–5. For Landsats 4 and 5, the Thematic Mapper (TM) sensor was also mounted. Landsat 6 was an upgraded version of its predecessors, carrying MSS and the Enhanced Thematic Mapper (ETM). However, it did not reach orbit. Landsat 7 was launched in

1999 with the ETM plus (ETM+) on board. While the satellite is active, its resulting scenes have missed approximately 22% of the data due to failure in the Scan Line Corrector since May 2003. The primary sensors on Landsat 8 are the Operational Land Imager (OLI) and the Thermal Infrared Sensor (TIRS). Though LULC information could be extracted from early images, temperature information retrieval was made possible in July 1982 when the TM sensor was introduced to Landsat 4 and others onward.

Table 2. Share of studies regarding the satellite data source used/study period considered categorized based on imagery resolution.

Spatial Resolution	Satellite/Sensor and Total Studies (%)			Use Per Study Period Length	
				Classification *	Total (%)
High resolution	All sources (13.6%) including IKONOS, SPOT, GeoEye, and QuickBird			Short	28.6
				Medium	42.9
				Long	21.4
				Very long	7.1
Medium resolution	Landsat Series (95.5%)	ASTER (4.5%)	HJ-1B (0.9%)	Short	22.4
				Medium	31.8
				Long	37.4
				Very long	8.4
Low resolution	MODIS (10.9%)			Short	25.0
				Medium	50.0
				Long	25.0
				Very long	0.0

* Study period length is classified based on the following: Short = [>10]; Medium [≥ 10 and <20]; Long [≥ 20 and <30]; and Very long [≥ 30].

Landsat data are popular among researchers for many reasons. First, the data have been provided at no cost since January 2009, when the USGS made all Landsat data free to the public (Landsat 7 data were made free in October 2008). Before that, a single scene's costs varied between \$20 and \$4000 [66]. This has been beneficial, especially for studies focusing on developing nations characterized by fast urbanization trends and population growth. Second, Landsat data are considered to comprise the genuine global archive that has constantly been updated for almost half a century following a strategy of regular imagery acquisition rather than the limited acquisition on images of interest or ready for purchase [66]. Third, the characteristics of the latest satellites and their imagery, mainly those related to spatial resolution, revisiting cycle, and swath dimensions (Table A1) (which are described as moderate), are convenient for most LULC and SUHI studies focusing on cities. Generally, one scene per city is needed. However, depending on the geographic location of some cities with regard to the path and row of the satellite, mosaicking multiple scenes may be required (see [67]). Fourth, the extensive use of Landsat imagery has been an incentive to develop well-documented techniques for optimal use.

MODIS: The second commonly used satellite imagery for LULC/SUHI studies is that of MODIS (10.9%). In general, MODIS data have been used in SUHI studies focusing on medium study periods (between 10 and 20 years) (Table 2) and/or seasonal variations. MODIS is an acronym that stands for Moderate Resolution Imaging Spectroradiometer. It is a NASA Earth Observing System (EOS) sensor that flies on NASA's Terra (1999) and Aqua (2002) satellites. Terra's orbit crosses the equator from north to south in the morning, and Aqua crosses the equator from south to north in the afternoon, providing worldwide coverage every 1–2 days. The EOS satellites have a scanning pattern of 55 degrees and orbit at the height of 705 km, with a swath width of 2330 km.

ASTER: ASTER imagery has been used in 4.5% of studies, making it the third most popular source. ASTER is another sensor mounted on the *Aqua* satellite launched into orbit in 1999. Given its capabilities, ASTER is usually used for nighttime analysis [54]. Satellite datasets of Terra ASTER level-1B contain radiometrically calibrated and geometrically registered data for all ASTER channels [54].

HJ-1B: Another imagery source used in the considered literature is HJ-1B, an optical minisatellite (2008) that forms the HJ-1 (Huan Jing = Environment) constellation along with another two small satellites—optical HJ-1A (2008) and radar HJ-1C (2012). The instruments onboard HJ-1B include two charge-coupled device (CCD) cameras and an infrared (IRS) camera whose spatial resolution range is between 30 and 300 m [68]. Although the minisatellite constellation is primarily designed for environmental monitoring and disaster risk assessment such as floods and forest fires [68,69], HJ-1B imagery was used to assess the relationship of LULC and SUHIs in [70].

4.2. LULC Classification: Types, Methods, and Indices

In this subsection, we shed light on the procedure of extracting LULC information from satellite data, focusing on (i) regularly adopted LULC classification schemes, (ii) LULC extraction methods including supervised and unsupervised methods, and (iii) indices used in tandem with LULC classification to identify the composition or configuration of target areas.

4.2.1. LULC Types

In the considered literature, authors often opted for different LULC classifications depending on several factors, including the geographical settings of the study area, the main focus of the study, and the quality of remotely sensed data. While the terminology used to depict each varies from one study to another, it was observed that the four classes most often present in most cases were UA, vegetation, water, and bare land.

In most cases, LULC types are defined based on the authors' or experts' knowledge of the geographic settings of the targeted area. In [71], for instance, the authors selected LULC classes as a result of consultation with an expert familiar with the city of Erbil to better assess the associations between LULC and LST. Another approach for determining LULC classes is to rely on the classification scheme provided by governmental or scientific agencies. For example, several studies focusing on Chinese cities used the land use classification system by the China National Committee of Agricultural Divisions dated back to 1984 [72] or by the Chinese Academy of Sciences (as in [73]). In comparative studies focusing on cities with similar characteristics (e.g., climate and landscape configuration) that are not necessarily located within the same country or region, authors have preferred to use a unified classification system such as the USGS 24-category land use categories. Fan et al., for example, used USGS 24 to compare the impacts of the spatiotemporal variations of LULC on UHIs in five desert cities located on three different continents (North America, Africa, and Asia) [5]. Additionally, there have been instances where authors used ready LULC classes based on inventories published by scientific agencies. An example of such an occurrence could be found in the study on the Polish city of Poznań [74], where the authors used the Europe-focused CORINE Land Cover inventory, with a total of 44 classes, updated and maintained regularly within the Copernicus Programme [75]. The same classification scheme was also followed in a comparative study of the effects of SUHIs in seven big Turkish cities [76].

A few studies were found to combine LULC types into few representative classes, as in [77], where the authors combined multiple LULC types into what they called “functional zones”. For instance, a functional zone labeled as “dense green space” was created as a result of the combination of several types of forests (indigenous, plantations, and thicket), water bodies, and wetlands. Besides the high multiplicity of LULC types and the small spatial extent of certain types, the main rationale behind this approach, according to the authors, was the similarity of the properties of the combined types. Huang and Wang opted for a similar approach by defining “urban functional zones” (UFZs), which are abstracted from typical LULC types to depict human activities [78]. On the other hand, it was observed that authors generally tended to expand typical LULC types to more representative classes to evaluate their impacts on SUHIs. For instance, vegetation classes were classified into several types based on their density [79,80] or types [79]. In the same

vein, urban development types were expanded to further understand the impact of different types of urban expansion on the worsening of UHIs.

In addition to typical LULC classes such as IS, vegetation, water, and cropland, Tran et al. classified urbanized areas into different categories to reflect their actual development types [80]: (i) infill, which refers to newly developed constructions surrounded by older built-up areas; (ii) extension, depicting new constructions intersecting with older built-up areas; and (iii) leapfrog development, describing new built-up areas separated from old UAs. The authors found that infill development exhibits the highest LST, followed by extension and (lastly) by leapfrog development, which is attributed to the high-LST LULC types surrounding infill and the good planning policies followed when constructing leapfrog UAs, which require proximity to public spaces such as parks and water bodies. It is evident that selecting convenient LULC classes for SUHI studies is a crucial step that might provide new insight and improve the understanding of the influence of different LULC types on SUHIs.

4.2.2. Extraction Methods

Pixel-, subpixel-, and object-based classifications have been used in revised studies using parametric and nonparametric methods. Though parametric methods, including the maximum likelihood classifier (MLC) and iterative self-organizing data analysis (ISODATA), are the most used, nonparametric machine-learning algorithms were found to have gained ground in recent SUHI-related publications. Such methods include support vector machine (SVM; [61,76,81–83]), random forest (RF; [81–85]), k-nearest neighbor (kNN; [81–83]), and neural networks (NNs; [81–83]). Nonparametric techniques present the advantage of being able to be used without a priori assumption on data distribution. This advantage has enabled researchers to evaluate several algorithms to determine which one has the highest accuracy scores. For instance, in [83], the authors compared four different classification techniques: SVM, kNN, RF, and NN. SVM outperformed all in terms of overall accuracy and kappa statistic. A similar approach and identical set of algorithms were employed in [81,82].

Regarding accuracy, studies relying on supervised methods have typically used a confusion matrix, also known as an error matrix, which encompasses statistics comparing the count of real samples and the corresponding predicted ones. Overall accuracy is the generally used metric to assess classification results, which correspond to the percentage of correctly predicted samples of all classes. Two other metrics reflecting the accuracies of different classes have also been calculated: the user's accuracy and the producer's accuracy [31,41,80,86–99]. Another measure used in tandem with the aforementioned accuracy metrics or alone is the kappa statistic [100], the values of which range between 0 and 1. The lowest values indicate slight to nonagreement between two datasets. In detail, according to Monserud and Leemans, values below 0.4 indicate poor or very poor agreement, values between 0.4 and 0.55 indicate fair agreement, values between 0.55 and 0.7 indicate good agreement, values between 0.7 and 0.85 indicate very good agreement, and values above 0.85 indicate excellent agreement between images [101].

For most studies, the minimum required for the overall classification accuracy was 85%, following the recommendations of [102,103]. More recent studies have applied an even stricter accuracy threshold of 90% for both overall accuracy and kappa statistic, as suggested in [104]. These demanding requirements may be attributed to the decreasing spatial resolution of recent remotely sensed data, along with the advancements of classification techniques. Nevertheless, it was difficult to reach such high accuracies in some cases. Fan et al., for example, employed an object-based classifier to perform eight-class LULC classification in five desert cities [5]. The authors succeeded in achieving accuracies superior to 85% for all three target years in the considered cities except for those of the Indian city of Jodhpur—which ranged between 80% and 82.57%. They attributed this relatively low accuracy to the complex spatial distribution of different LULC classes alongside the similarity of spectral responses in several of these classes. For this reason, unsupervised

classification is usually first conducted by using satellite data to determine the spectral separability of the LULC classes [54]. Unsupervised methods include ISODATA alone or as a hybrid method with a supervised algorithm [105]. The initial use of a hybrid approach initially allows authors to gain insight into the number of major spectral differences [77]. Other studies have solely relied on an unsupervised approach [92,99,106].

Samples for validation purposes have been collected through field surveys using GPS [54,93,107,108] and aerial photos [51,72], as well as being extracted from the commercial imagery of high-resolution satellites such as IKONOS [58,109], SPOT [51,52,63,72,107,110,111], QuickBird [20,58], GeoEye [111], and GaoFen-1 [112] provided by private companies. However, researchers are moving away from these methods for several reasons. First, fieldwork is a time- and budget-consuming task that requires hefty effort. Second, high-resolution images are costly, which has led to issues related to the availability of historical data in many regions in the world. In recent years, however, the free-of-charge Google Earth has offered a reliable alternative for these traditional sources to extract balanced validation points using sampling techniques such as stratified random sampling [76,99,113–115].

4.2.3. Indices as LULC Proxy

The use of indices calculated from different sensors bands or other indices was found to be common in the reviewed literature. Authors have used these indices to further assess the relationship between LST and different characteristics of target areas including biophysical properties, landscape composition and/or configuration, and (less frequently), an alternative approach to the supervised/unsupervised methods for extracting LULC types. Table A2 lists the most employed indices in the reviewed studies, as well as the proportion of each category of indices. Broadly, the employed indices were found to fall into five categories: vegetation, built-up, water, bare land, and landscape metrics.

There are several vegetation-related indices. However, the normalized difference vegetation index (NDVI) and fractional vegetation cover (FVC) remain the most employed indices, accounting for 52.5% and 8.2%, respectively, of SUHI research. The NDVI has been solely used to extract emissivity values for LST retrieval (Section 4.3.1) in several studies; as a result, these studies were not included in this analysis. A few other studies relied on the soil-adjusted vegetation index (SAVI), transformed difference vegetation index (TDVI), and enhanced vegetation index (EVI), which were used together only in 4.5% of reviewed studies.

The built-up indices were found to be second in terms of frequency of use in the reviewed studies. While several new indices, including the enhanced built-up and bareness index (EBBI), index-based built-up index (IBI), and normalized difference impervious surface index (NDISI)—accounting for 2.7%, 0.9%, and 0.9%, respectively—have been introduced in recent studies, the normalized difference built-up index (NDBI) was employed in almost 24.5% of studies to represent built-up areas. Water was mostly represented by the modified difference water index (NDWI) in about 7.3% of studies, followed by the modified normalized difference water index (MNDWI) with a share of 6.4%. Of the studies, only 0.8% relied on the land surface water index (LSWI) and normalized difference moisture index (NDMI) each. Two indices were used as proxies of bare lands: the normalized difference bareness index (NDBaI) and dry bare-soil index (DBSI), which were found to account for, respectively, 4.9% and 2.1% of studies. Landscape metrics, both compositional and configurational, were employed in approximately 5.7% of studies.

4.3. SUHI Calculation Methods

In this subsection, we shed light on the approaches employed in the considered literature to quantify SUHIs. The approaches roughly fall into two categories: the first consists of methods using retrieved LST as a proxy, and the second is based on the calculation of SUHI intensity defined as LST differences between UAs and less developed areas (e.g., rural). Numerous studies combined both approaches. Though LST retrieval is a critical step in the process, a detailed description of the different methods used is beyond the scope of this

review. Instead, the reader is referred to a published review by Li et al. for a comprehensive summary of the methodologies and algorithms developed for LST retrieval [116].

4.3.1. LST as a Proxy of SUHI

LST is regarded as the land surface's radiative skin temperature [117], which is considered a key element in the physics of the land surface through energy and water exchanges with the atmosphere [109]. Though LST is believed to be more adequate for quantifying UHIs at urban canopy layers [6], SUHIs tend to follow the same patterns as AUHIs according to several previous studies [118–120]. In most of the considered literature, LST was used as the sole proxy of SUHIs to analyze their spatial variability concerning different LULC classes, which can be attributed to the fact that LST is highly correlated with surface properties [121]. Chen et al., for instance, classified the retrieved LST information into five categories (very low, low, medium, high, and very high), reflecting its magnitude, based on the deviation from the mean value [112]. The relationships between LST and different LULC data are further detailed in the following section. In this section, an overview of the methods of LST retrieval from satellite thermal data is presented as a critical step in the reviewed literature.

The retrieval of LST from satellite thermal data is a complex but critical procedure in SUHI studies. Its complexity resides not only in the multiple processes that are involved, including radiometric sensor calibrations and the required adjustments for air and surface emissivity [109] but also in the number of parameters that need to be accurately known, such as emissivity transmittance and atmospheric temperature [114].

In general, efforts to retrieve surface temperature (ST) from the thermal data of satellite sensors have been made since the late 1960s, when Anding and Kauth introduced a method known as the split window (SW) that was capable of estimating sea surface temperature [122]. Since then, numerous attempts were made to extend the SW technique to obtain LST before the algorithm was extended to be able to retrieve it [123,124]. A wide range of other algorithms and techniques have been additionally proposed to retrieve LST.

According to Li et al., LST-retrieval methods fall into three broad categories depending on whether land surface emissivity (LSE) and atmospheric quantities are known [116]: (i) retrieval methods with known LSE including single-channel (SC) algorithms, multichannel (MC) algorithms, and multiangle algorithms; (ii) retrieval methods with unknown LSE including the classification-based emissivity method (CBM) and NDVI-based emissivity methods (NBEMs); and (iii) retrieval methods with unknown emissivity and unknown atmospheric quantities. Among these methods, SC algorithms, characterized by their simplicity, were found to have been widely used in the reviewed literature. As their name suggests, they are used to extract LST from the thermal data of sensors with a single TIR channel (e.g., Landsat 4–5 (TM) and 7 (ETM+)).

Various variants of the single-channel method have been proposed, notably the algorithm (often referred to as the mono-window algorithm (MWA)) specifically developed for the thermal band of Landsat 5 TM channel 6 by Qin et al. [125], which was applied in multiple reviewed studies [14,94,112,114,126,127]. The MWA generally requires three parameters: emissivity, transmittance, and effective mean atmospheric temperature [112]. Jiménez-Muñoz and Sobrino developed a universal single-channel (USC) algorithm capable of retrieving LST from any TIR channel requiring two parameters, such as atmospheric moisture content and emissivity [128]. Similar to the MWA, the USC algorithm has been applied in the considered literature across different cities [45,111]. SC algorithms, however, are limited in their applicability due to a variety of criteria that have been deemed difficult, if not impossible, to meet—notably, the a priori knowledge of the emissivity of each pixel [116] and detailed information about atmospheric profiles during the satellite overpass of a given target area [51,116]. In contrast to SC algorithms, MC algorithms, known as split-window algorithms, have been employed to retrieve LST from sensors with multiple adjacent thermal bands, including Landsat 8 TIRS, ASTER, and MODIS without the need for accurate atmospheric profile data at acquisition time.

4.3.2. SUHI Intensity

SUHI is the second most common approach that has been used to quantify SUHI magnitudes in cities. Generally, SUHI is the difference between retrieved LST means calculated in UAs and their surroundings, often underdeveloped, including suburban or rural areas. The boundary that has to be established to distinguish between the two regions is problematic to define. Broadly, two methods have been employed in the literature.

The first heuristic approach relies on city features such as traffic rings, administrative boundaries, and buffer zones. In a Shanghai-focused study [51], the authors divided the target area into three sublevels based on the inner and outer traffic rings surrounding the city: (i) the city proper located within the inner traffic ring, (ii) a periurban area within the inner and outer traffic rings, and (iii) a region beyond the outer traffic ring, which is a rural area with low-to-moderately dense residential areas, farmland, and natural surroundings. After considering this layout, the authors calculated seasonal and interannual variations of two SUHI intensity indices: the first was between the city center and surrounding rural areas, and the other was between urban fringe and surrounding rural areas. A similar approach has been employed in other cities such as Jinan city [107] and Fuzhou city [72]. Another way to delineate urban and rural areas found in the literature consists of using administrative boundaries [129]. Buffer zoning while centering the city core is an alternative approach found in the literature to extract urban/rural areas. Rasul et al. defined rural areas with a 10 km buffer zone beyond the city core [71]. However, the authors did not report how the core was delineated. It should be noted that this approach was applied to an arid city with outskirts characterized by quasi similar land cover classes. Nonetheless, these heuristic approaches might not be suitable for studies focusing on the decadal monitoring of SUHI due to major changes in landscapes.

Other studies have opted to rely on LULC classification as a way to differentiate urban- and nonurban-labeled pixels. Ultimately, the LST means of areas classed as nonurban are subtracted from areas identified as nonurban, including vegetation (grass, forest, etc.) and bare land. Numerous studies were found to have followed this approach [130,131]. Following the same concept, other studies employed ISs as proxies of UAs, and rural areas have been represented by green space (GS) in most cases. This approach was applied, for instance, by Estoque and Murayama to calculate the SUHI in the tropical mountain of Baguio, Philippines [12]. The authors calculated the SUHI as the mean LST difference between ISs and GSs. Furthermore, in an attempt to replicate the concept of the inter-zone UHI intensity comparison proposed in [132], which involves an initial classification of the landscape into urban or local climate zones followed by inter-zone temperature differences, the authors distinguished two types of GS in addition to IS: a GS1 that includes forest and shrubland and a GS2 that includes grassland and cultivated land. Subsequently, the SUHI magnitude between the IS and other zones (GS, GS1, and GS2) was calculated. The same approach was applied in Kandy City, Sri Lanka [83].

4.4. Relationship Assessment of LULC and SUHIs

Various methods have been employed to assess the relationship between LULC changes and SUHI changes. Some studies used more than one method for the analysis, either for comparison or validation purposes.

Regression analysis tops the list with approximately 20.9% of manuscripts. Ordinary least square (OLS) regression has been used more frequently to characterize the relationship between LST and LULC based on several indices presented in Section 4.2.3. Though popular among researchers, OLS estimators present a major limitation; according to Deilami et al. [133], they do not account for spatial variability, which leads to issues associated with spatial autocorrelation and nonstationarity. Due to this limitation, the geographically weighted regression (GWR) was used in several studies as a potential alternative to counter OLS limitations. In GWR models, the spatial variability between the response variable (LST) and explanatory variables (e.g., indices and other factors detailed in Section 4.5) is taken into consideration. A GWR model generates estimates for every point

in space based on local linear regression estimators that depend on a subset of information from neighboring points [134]. Although it was found that GWR models outperform OLS models in multiple studies [108,133–135], both procedures have their own benefits. In contrast to GWR, which is more effective at the local level, OLS has been found to aid in quantifying the impacts of various factors of SUHIs at the regional level [133,134].

Chart analysis, which relies on the zonal statistics method and is presented in the form of charts to illustrate the relationship between LULC and SUHIs over time, was found to come second (19.8%). Among the selected papers, 11 analyzed the mean LST for each LULC category and compared the LST change in different years. Overall, the trend of mean LST was found to be increasing in all LULC categories, and the built-up always had the highest LST among all LULC categories [54]. Moreover, vegetation coverage is an essential factor that can help cool cities and reduce the impact of LST. However, the benefit of vegetation has not been given sufficient attention. For example, the percentage of vegetation was found to have decreased from 6.3% to 1.9% over 25 years in Shiraz city, Iran [136]. At the same time, the mean LST of vegetation changed from 35.1 °C in 1993 to 39.5 °C in 2018, which proved that the cooling power of vegetation was affected by the total quantity. More accurate analyses would help to better identify the impact of different LULC types on LST. For instance, some authors plotted the space lattice of the LST, NDVI, and LULC, and the results showed that the LST values of water and green spaces were lower than those of built-up and cropland spaces [137].

Correlation analysis was found to be the third most common method (8%), and it has often been used together with regression analysis. We distinguish three types of correlations used in reviewed studies: (i) Pearson correlation, (ii) Kendall rank correlation, and (iii) canonical correlation analysis. Pearson correlation was used in most of the studies [11,45,52,97,99]. Only two studies opted for the other two types. Lo and Quattrochi used both canonical and Pearson correlations analyses to investigate the relationship between LST spatial patterns and those of volatile organic compounds (VOC) and nitrogen oxide (NO_x) emissions in Atlanta, US [31]. Kendall rank correlation was used in [5] to detect the monotonic dependence between SUHIs and relative urban-rural vegetation differences—a metric that measures the difference of NDVI means in urban and rural areas—concerning the populations and UAs of five desert cities. The authors argued that Kendall's coefficient offers resistance against outliers and missing values in addition to its capability to identify any type of monotonic relationship—not just linear dependence, as measured by the Pearson coefficient.

Calculating the contribution index (CI) was found to be another common approach (8%) used to evaluate the impacts of different LULC types on LST variations. The CI measures the thermal contribution of various LULC categories on the LST by multiplying the proportion of a given LULC type to the entire study area by the difference between the mean LST of the LULC type in the question and that of the whole study area. Positive CI values of an LULC type indicate a direct influence on enhancing SUHIs, whereas negative values indicate a negative effect on SUHIs [138]. The index was first employed by Chen et al. to assess the impact of 10-year LULC spatiotemporal changes on SUHIs at a regional-scale level in the Pearl River Delta located in Guangdong Province and a city-scale level in Shenzhen city [87]. It was then used in multiple studies in different research areas, including Shenyang, China [94]; Ethekewini, South Africa [77]; Wuhan, China [139]; Malda, India [138]; and Delhi, India [55]. Based on the obtained CI values of different LULC types, Pramanik and Punia further calculated another index called the landscape index (LI), defined as the quotient of the CI of SUHI sink (i.e., croplands, vegetation, and water bodies) and source (i.e., built-up, fallow, and bare lands) landscapes [55].

Though fewer, other noteworthy methods such as the ANOVA test [61], the crossover comparison method [12,83], grid-level analysis [11], centroid movement analysis [45,140], temperature vegetation index space [55,141], and hot-spot analysis [80] have also been used in studies.

1984 to 2015 as a result of a heavy urban expansion and vegetation cover loss [143]. In mountain cities, identical tendencies were also observed. Increases in SUHI were reported, for instance, in Baguio (+0.7 °C between 1987 and 2015) [12] and Kandy (+2.3 °C between 1996 and 2017) [83].

The resulting LULC spatial structure has been found to predominantly affect the spatial patterns of the recorded LST and to intensify SUHI effects [80]. By examining various studies carried out in different cities across the globe, we compiled a list of the LULC types with considerable influence on SUHIs including ISs/UAs, vegetation, water bodies, and seasonal variations.

- IS/UA: UAs, along with pavements and road networks, form ISs. A substantial body of research points to the fact that ISs have strong warming effects in cities [20], regardless of the reigning climate (tropical, desert, etc.) or the geographical settings (topography, elevation, etc.). While some studies have focused on ISs, others have separately investigated the effects of UAs, roads, and pavements on UHI. However, both sets of studies concluded that the highest LST values are exhibited by either UAs or ISs [11,14,41,45,72,74,80,97,111,112,115,126,133]. Regarding association, it has been found that both ISs and UAs have strong and significant linear positive correlations with LST [80,87,99,112] during all seasons [97]. This is attributed to the fact ISs absorb more solar radiation and have greater thermal capacities and conductivities, allowing heat to be retained during the day and released at night [143]. Ultimately, urban expansion exacerbates this process. Tran et al. estimated that a 1% increase in UAs in the Hanoi inner city could raise the surface temperature anywhere between 0.075 and 0.108 °C [80]. Urban expansion, however, does not only concern the size of UAs (i.e., footprint areas), due not only to their low albedo roofing materials (e.g., concrete and asbestoses)—as observed in [11,33,106,113]—but also the buildings' heights [56,76], UA density [112], porosity (defined as the ratio of total open space to total built-up areas [133]), and UA development level [74]. Another IS component, which consists of pavements such as parking lots and harbor jetty covered with dark materials such as asphalt, was found to be a significant contributor to UHIs [33]. Roads, on the other hand, have been found to increase SUHI impacts in two ways: first through their paved surfaces that absorb shortwave radiation and store heat throughout the day and release it slowly at night [99] (similarly to other pavements) and second via emissions produced by traffic passing through them.
- Vegetation: In contrast to ISs, vegetation absorbs solar radiation and removes a great amount of stored heat via evapotranspiration—a process that releases water vapor into the ambient air and subsequently contributes to cooling surrounding areas [11,12]. The relationship between LST and vegetation cover is complex. It depends on many considerations related to the study area (e.g., seasonal variations and landscape topography) and the characteristics of the vegetation cover itself (e.g., the nature of species, heights, and density). Numerous studies in the reviewed literature reported a negative linear relationship between LST and vegetation, as quantified through multiple indices (refer to Section 4.2.3 for a detailed list), most notably the NDVI [11,45,53,87,88,98,111,126,136,144–149] and FVC [53]. Rotem-Mindali et al. even found an exponential relationship between the NDVI and LST [150]. A few other studies reported negligible correlation due to various possible causes. Rasul et al., for instance, found a weak yet significant inverse relationship between LST and the NDVI during the summer season in the city of Erbil, Iraq, which is characterized by a temperate climate [71]. After considering seasonal variations in the Chinese city of Jinan, Meng and Liu concluded that FVC is negatively correlated with LST during all seasons except for winter [107]. Likewise, Wang et al. argued that variations of seasons were a possible cause of their obtained weak correlation between LST and the NDVI in Shanghai [20]. After exploring the reviewed case studies, however, it became evident that a fast rate of urban expansion to the detriment of vegetation cover leads to the weakening of the impact of vegetation on LST in comparison to the influence

- exerted by ISs. This can be concluded from the weak correlation between LST and vegetation when compared with LST and ISs, as reported in [20,96].
- Water: As with vegetation, water bodies have a cooling effect due to their ability to absorb heat and release it in the form of water vapor, leading to lower ambient temperatures in their vicinities. In an investigation of the Chinese city of Wuhan, in which water accounts for over 25% of the total area of the central district—including two rivers (the Yangtze River and Han River), East Lake (the largest urban lake in China), and dozens of other lakes—Wu et al. found that both the area and the spatial distribution of water bodies contributed to significant distributions in the effects caused by SUHIs [70]. Moreover, the findings reported in multiple studies have affirmed that water bodies exhibit the lowest LSTs [11,20,41,45,47,60,73,78,79,88,90,93,97,98,111,112,115,138,139,151–153], along with vegetation cover. Furthermore, water has generally been found to have a negative correlation with LST [20,111,154], except for a few circumstances due to various reasons primarily related to the climate characteristics of cities. For instance, in [99], the authors attributed the lack of a significant relationship between LST variations and water bodies' changes that occurred in desert city Phoenix between 2000 and 2014 to the scarcity of large and evenly distributed open-air water bodies in the target area, along with possible LULC classification errors. In comparison with vegetation, water usually has a less significant association with LST [20].
 - Seasonal variations: Seasonal variations have significant impacts on the spatial and temporal distribution of SUHIs. While the bulk of research has focused on interannual variations, seasonal fluctuations were also taken into account in several manuscripts, particularly in those with short study durations (less than 10 years). An illustration of such investigations was reported in [107], where the authors analyzed SUHI variations in all seasons for the Chinese city of Jinan. Based on LST data derived from Landsat images acquired between 1992 and 2011, they calculated two SUHli indices (while considering rural areas) based on the two traffic rings surrounding Jinan urban center. Their findings showed that both SUHli indices were stronger during summer (0.98–1.75 °C) and spring (0.40–0.85 °C) and weaker during autumn (0.16–0.37 °C) and winter (from −0.05 to −0.03 °C). These results are aligned with those reported in [52] for Shanghai. In the tropical Indian city of Delhi, Sharma and Joshi also found that summer had the maximum SUHli (16.2 °C), followed by monsoon and spring seasons with SUHli values of 13.8 and 12 °C, respectively [22]. On the other hand, the post-monsoon and winter seasons exhibited the lowest SUHli values of 10.5 and 7.4 °C, respectively. The dominant factors impacting SUHI levels depend on seasonal changes. For instance, Zhang et al. determined that water, vegetation, and developed lands are the major drivers during all seasons except for summer in Shanghai [52]. These results partly agree with those reported in [77], where the authors found that the functional zone “dense green spaces” (including different types of forests, water bodies, and wetlands) in Ethekwini, South Africa, had a major heat contribution in the autumn, winter, and spring seasons. On the other hand, Song et al. reported that ISs had higher mean LSTs during all seasons except for winter in the Chinese temperate city of Hangzhou [155].

4.5.2. Landscape Composition and Configuration

In addition to LULC's different types and their dynamics, several studies have analyzed the relationships between urban climate and landscape patterns. A wide range of metrics has been developed to characterize these patterns and relate them with ecological processes [156]. As described in Section 4.2.3, these metrics can be categorized into two general groups: compositional and configurational. Metrics for landscape composition assess the existence and quantity of various patch types in the landscape without specification on its spatial characteristics, whereas those for landscape configuration measure the spatial distribution of patches within the landscape [50]. An illustration of such investigation was reported in [50], the authors analyzed the impacts of landscape structure on SUHIs in the

Shanghai metropolitan area in early spring (March 2001) and summer (July 2001). Eight landscape metrics—compositional (PLAND, SHEI, and SHDI) and configurational (ED, PD, LSI, CI, and CONTAGION)—were selected to investigate the relationship between LST and landscape patterns with regard to the LULC types of residential, public facilities, industrial, traffic, green land, water, agricultural, and other land uses including under-construction sites, cemeteries, and historic relics. High correlations were found between LST and landscape metrics for residential and urban green, with significant fluctuations observed due to alterations in SUHI spatial configurations induced by seasonal changes affecting vegetation patterns. Furthermore, residential areas' contributions to LST were found to be significantly influenced by their morphological characteristics. High-rise residential areas were found to have lower LSTs than low-rise residential areas for many reasons. First, low-rise residential zones have more horizontal active surfaces than high-rises. Second, smaller structures with lower thermal inertia produce shorter shadows than high ones. Third, when wind speed rises with height, the lower boundary layer's aerodynamics vary considerably. As a result, high-rise structures have a greater aerodynamic conductance than low-rise ones. Finally, the temperature of the lower boundary layer drops with height. The top of the high rise is cooler than the bottom. The proposed methodology was further expanded in [78], where the authors selected 2D and 3D building metrics related to shape, arrangement, composition, and distribution (in addition to landscape metrics) to evaluate the association between SUHIs and 2D/3D urban morphology in Wuhan, China. Two functional zones were considered: built-up (including residential, industrial, commercial, open space, and public services) and non-built-up (including urban green areas, agricultural lands, forests, rivers, and lakes). The findings of the study can be summarized as follows: (1) during the summer daylight, four LULC classes, namely buildings, other ISs (e.g., pavements, open areas, and squares), grass/shrubs, and trees, have significant effects on intraurban LST variation at a fine-scale; (2) the proportion of trees is the primary element affecting LST cooling via evapotranspiration and shade casting; and (3) during summer daylight, 3D urban morphology has an effect on LST, although the correlations are not as tight as those for 2D urban morphology. It was found that the most significant 3D metrics are the mean height (MH) and the sky view factor (SVF)—a metric measuring the extent of 3D open space that ranges from 0 (no sky in sight) to 1 (no obstacles in sight). A negative correlation was found between MH and LST in summer, indicating that high-rise buildings may help counteract SUHIs throughout the day. The SVF impact on LST is complex because it depends on the surrounding environment and relates to enhancing air circulation in the case of a higher SVF and reducing incoming solar radiation in the case of a lower SVF.

4.5.3. Terrain Characteristics

Generally speaking, most of the investigated cities in the reviewed literature are located in flat areas with slight or barely noticeable topographic variations. For that reason, few researchers have considered topography-related factors. On the other hand, researchers who focused on mountain cities or those dotted with varied landscapes concluded the importance of topography in understanding the spatial variability of LST. In a study that focused on exploring the spatial variations of LST between 2000 and 2010 in the tropical Malaysian capital Kuala Lumpur, Amanollahi et al. concluded that its elevated landscape plays a significant role in stabilizing the heat island in the city in two ways [142]. First, the expansion of ISs has resulted in fragmented vegetation cover—mainly consisting of forests in the study area—which has led to increases in surface temperatures; second, forests located at high elevations were recorded to have the lowest temperatures. The rise of LST due to fragmented forests had been somewhat regulated by the low LST recorded in high-elevated forests, resulting in the highest standard deviation of LST values of any LULC type. Second, the Titiwangsa mountain range with peaks over 2500 m above sea level (asl), located to the east, northeast, and north of the city, acts as a dam that stops winds coming from the north and east from blowing in the directions toward the city which, according to the authors, stabilizes the heat island in Kuala Lumpur. These findings

relatively correspond to those reported in [157], in which the author partly attributed the lowest LST values observed in forests to their highest altitudes in the Czech city of Brno. Even in cities with a dry climate and relatively low landscape, such as Cairo, topography has been deemed a key factor influencing LST [106]. The author found that the mean LST at the highest region, El-Mokatam Plateau at 500 m asl, was 37 °C in comparison to the 39 °C value recorded at 100 m—which indicates an LST increase of 0.5 °C for each 100 m elevation. In the tropical mountain city of Baguio, the Philippines, Estoque and Murayama investigated the effects of topography on UHIs through additional parameters including elevation, slope, aspect, and hill shade [12]. Empirical analysis showed that these parameters, together with those of landscape composition, were capable of explaining a great deal of LST spatial variability in three different years of 1987, 2001, and 2015.

4.5.4. Socioeconomic Factors

Though relatively limited in occurrence, socioeconomic factors have also been considered as potential variables that contribute to elevated LST in cities, especially from the perspective that anthropogenic activities of residential, industrial, and/or commercial natures are responsible for enhancing surface temperatures.

- Population density (PD): PD has been introduced in several studies as a factor impacting SUHIs. For example, Zhang et al. investigated the links between PD and SUHIs in Nanchang, China [115]. The authors found significant positive correlations between PD and mean LST in 2000 and 2013, concluding that as PD increases, LST also increases. This result is consistent with that found in other studies carried out in different cities such as Wuhan [129], Fuzhou [72], Brisbane [133], Shanghai [45], Zhengzhou [73], and Hefei [158]. However, a PD-induced LST increase does not concern the total number of people located in a given area as much as it is related to the socioeconomic activities carried out by people daily in houses or places of work (e.g., industrial centers) [115]. This was confirmed in [129], where the authors concluded that, in contrast to PD variations that have been found to be somewhat correlated with LST, Wuhan population changes from 2000 to 2009 had no direct relationship with LST.
- Other socioeconomic factors: Our investigation shows that socioeconomic factors are often overlooked, generally because of a lack of data. Nevertheless, several researchers introduced such variables and assessed their impact on SUHI development. These include (i) emissions such as those of VOC and NO_x [31], waste gas emissions [46], and carbon dioxide (CO₂) [115]; (ii) electricity [76,96]; (iii) employment density [61,133]; (iv) night light [45]; (v) gross domestic product (GDP, [46]); and (vi) house rent [159].

4.6. An Overview of Proposed Mitigation Strategies

In light of the findings of the reviewed studies, the magnitude of SUHIs can be said to be associated with rapid urban sprawl to the detriment of green areas. Several suggestions have been proposed in the literature to alleviate SUHI impacts. We present a compiled list of the main strategies suggested:

- Promoting greenery: Implementing policies encouraging more green areas [11,73,99,115], preferably within the urban premise and beyond, is one of the most suggested SUHI mitigation strategies given that increases in SUHI magnitude are highly associated with depletion of vegetation cover. Within UAs, greening concepts need to be implemented in both the horizontal and vertical directions [82]. Kleerekoper et al. described four forms of vegetation that can be fostered: parks, trees along streets, green in private gardens, and green roofs or facades [160]. Regarding the cooling effect, Wong et al. reported that ground greenery often lowers the surface temperature by 2–9 °C, whereas roofs or buildings walls covered with green layers reduce surface temperature by approximately 17 °C [161]. Additionally, the type of planted vegetation makes a great difference in cooling effects. For instance, Zhang compared the cooling effects of five

regionally common shrubs in Guangzhou, China [162]. According to the author, only one vegetation type, *Murraya exotica* L., showed excellent cooling effects. Furthermore, various studies have emphasized other parameters deemed critical for maximizing SUHI mitigation gains, including park shape [110,161], park size [110,161], and plant placement [161]. Thus, such considerations need to be considered by urban planners prior to implementing a strategy for optimal outcomes in the long run. Beyond UAs, the use of greenbelts surrounding cities is an effective way to combat SUHIs. In [94], the authors demonstrated the cooling effects of the greenbelt surrounding the Chinese city of Shenyang based on an investigation of LULC changes on SUHIs from 1986 to 2007, although this effect had started to fade because of urban sprawl. In desert cities, greenbelts are highly recommended, as seen in [106], where the authors recommended expanding greenbelts to protect new urban communities in the Cairo metropolitan area against SUHIs amplified by air pollution caused by dust and suspended aerosols.

- Safeguarding water bodies: Similar to vegetation, the reviewed studies reported that changes in water bodies had had substantial effects on SUHI mitigation [50,87,163], concluding that alleviating SUHIs necessitates safeguarding water bodies. In Wuhan city, Wu et al. found considerable spatial variations in SUHI effects, which they attributed to water bodies' distribution [70]. In a study carried out on the tropical city of Kuala Lumpur, Amanollahi et al. recommended increasing the number of retention ponds and adding new vegetation areas [142]. Among various advanced materials and techniques, Cai et al. suggested using waterscapes in the city of Fuzhou to counter the impacts of SUHIs [72]. While it has been reported that the impacts of water bodies on SUHIs are generally less effective than those of vegetation cover [164], combining both approaches would be a good strategy to reduce SUHI impacts.
- Using cool roofing/paving materials: Though the increase in green and blue areas may be feasible in cities under moderate climates (i.e., temperate, tropical, and continental), such measures are difficult, if not impossible, to implement in desert cities due to scarcity of water resources, as reported in the case of Phoenix [99]. Reducing ISs' properties to absorb solar radiation by using reflective materials [11,33,165] is an alternative option in cities with harsh and moderate climates alike. That can be conducted using highly emissive materials to prevent heat retention and by painting roofs and pavements with white paint [11].
- Other notable measures: Regarding LULC changes, the aforementioned measures have been the most suggested ones in the reviewed literature to alleviate SUHIs. A few studies suggested other ways such as (i) relying more and more on renewable energy (e.g., solar and wind) at the expense of fossil-fuel-based energy to reduce carbon emissions [11] and (ii) promoting incentive programs such as "carbon credits" targeting polluting companies to reduce emitted anthropogenic gases [11].

In summary, mitigation measures depend on the characteristics of the target area, mainly in terms of the reigning climate, local topography, size, and geographical settings. It is worth noting that this review only covers commonly suggested mitigation strategies in the considered literature. Policy and technology responses developed for the alleviation of UHI impacts are not discussed. For more information, one may refer to a study by Kleerekoper et al. [160] or a recent and more focused review conducted by Degirmenci et al. [39].

4.7. Limitations and Future Directions

In this subsection, the limitations or obstacles facing studies focusing on the associations between LULC spatiotemporal changes and SUHIs are discussed. This is followed by the proposed future paths that such a topic may be directed toward.

4.7.1. Limitations

Though studies focusing on the historical trends of SUHIs in relation to LULC changes have helped our understanding, several critical limitations have been pinpointed in the

reviewed literature and need to be addressed in future research. These limitations concern the used data, executed methods, or a principal combination of both.

Perhaps the biggest challenge that limits such studies is the incapacity to validate satellite-derived LSTs using in situ measurements collected from field surveys or historical data collected via climatological station networks. The lack of such networks in targeted areas and the time- and budget-consuming fieldwork are the main obstacles that have hindered the validation process of satellite-derived LSTs in numerous case studies. The deployment of reliable networks usually comes with huge expenses, as it requires continuous maintenance. Even when available, in situ records may be incomplete due to various reasons, such as the forced relocation of stations (as reported in [144]), which makes them inadequate for studies focusing on the long-period monitoring of SUHI and LULC changes. In addition, high costs or privacy barriers may hinder researchers from accessing such valuable data. Nevertheless, numerous researchers have been able to confirm small differences between SUHIs and AUHIs, as illustrated in [54], where the authors found an error of 2–3 °C between satellite-derived mean LSTs and average temperatures based on in situ measurements. Error fluctuations were found to vary depending on the LULC type, while vegetation averaged 28.7 °C based on field measurements and 30.8 °C based on estimation via satellite data; UAs averaged 30.1 °C based on field measurements, and satellite estimations indicated 32.7 °C. In the city of Zhengzhou, quasi-identical results were described by Min et al., who found differences ranging between 2.7 and 4.7 °C, based on historical meteorological data [73]. Similarly, using records from four climatological stations, Nguyen et al. found that these differences varied between 0.3 and 3.34 °C, with higher differences observed in UAs and lower differences observed in rural areas [96]. A different approach was used in [22], where the authors conducted a field survey intending to collect over 200 ground observations across Delhi during the spring season. A high correlation (0.89), along with a relatively high coefficient of multiple determination ($r^2 = 0.79$) and quasi-equal standard deviation (0.72 °C), was reported between the two sets, thus indicating that the LST estimated from satellite thermal sensor data was as precise as those measured in situ. These findings are partly aligned with those reported in [97], in which the authors found a significant correlation between air temperatures (measured at 137 sites) and satellite-estimated LST during the winter (January 2014) and pre-monsoon (April 2014) seasons in the city of Malda. Aside from validation using meteorological station data or field survey measurements, LST data retrieved from satellite sensors have been used for comparison against each other. This was described in [126], where the authors used the MODIS LST product to validate LST estimated from Landsat imagery in different years (2006, 2009, and 2016). Empirical analysis showed the existence of moderate-to-strong correlations ranging from 0.44 and 0.55 between the LST estimated from Landsat (5 TM and 8 TIRS) and MODIS. According to Swain et al. [166], the refined MODIS LST products were reliable because they had already been validated using ground observations; they cited [167] as a reference paper where the authors demonstrated that their accuracy was better than 1 K in 39 out of 47 cases, with all 47 cases having a root mean squares of differences less than 0.7 K. A similar approach was used by Chaka and Oda to validate Landsat 8 TIRS data in the city of Hawassa, Southern Ethiopia [79].

A second limitation observed in the reviewed literature is related to the limited number of dates that were considered for analyzing the links between SUHIs and LULC changes, especially those monitoring long periods. This might hinder the provision of a true picture of the trends of the impacts of different LULC changes on SUHIs in cities during such a long timeframe, specifically those related to seasonality [22] or the occurrence of rare abnormal events (e.g., drought and cold waves) that might lead to misleading interpretations. A study by Feng et al. in Xiamen city, China, revealed that a cold wave that occurred in 1992 may have been the cause behind water bodies exhibiting the highest LST that year, despite being one of the coolest LULC types in other years (1987, 1997, and 2007) [121]. Moreover, in [111], the authors partly attributed the high temperature recorded in 2015 observed in the mountain city of Yan'an city, China, to the significant climatic impact

of the global El Niño phenomenon. Another rare event impacting SUHIs was described in [166], where the authors reported an unusual increase in MODIS-derived mean LST recorded in 2009 in agricultural lands, which resulted in a small difference between rural areas and UAs. These anomalies were attributed to the severe drought that affected the region in 2009, which impacted the vegetation cover and soil moisture content. From this perspective, while it requires massive efforts and resources, relying on imagery data with higher temporal frequency to monitor interannual [83] and seasonal [22] SUHI variations is highly recommended because it would improve our understanding of the impacts of LULC spatial and temporal changes and prevent misleading interpretations. An example of such investigations was illustrated in [168]; using 507 Landsat images, the authors analyzed historic LULC changes—which occurred in Atlanta between 1984 and 2011—and explored their effects on thermal landscape patterns.

The third challenge that faces SUHI/LULC studies is related to the quality of archived remotely sensed data. It is evident that multiple data sources are available, as presented in Section 4.1, which have allowed researchers to carry out studies in different cities across the globe. However, a serious limitation that impedes the use of satellite data is the high percentage of cloud cover, notably in tropical regions. This issue was illustrated in [114], where the authors described cloud coverage as a “curse” for optical remote sensing following their struggle to find Landsat data of the Kuala Lumpur metropolitan city with minimal cloud cover. Subsequently, the authors could finally collect images during the summer seasons of five years between 1997 and 2013, covering percentages ranging from 4% to 24%. In the same study area, Amanollahi et al. found the same issue regarding the collection of cloud-free Landsat imagery, leading the authors to somewhat limit their investigation of SUHIs to only two dates (1990 and 2006) [142]. Though the two collected images were over 95% cloud-free, the authors noticed that 90% of clouds were clustered above the vegetated area, leading the authors to classify them as vegetation. Clouds not only contribute to less accurate LULC classification [142] but also affect the estimation of LST. This was further detailed in [169], where the authors used over 80 Landsat images to monitor SUHI evolution in the tropical metropolitan area of Rio de Janeiro between 1984 and 2015. It was found that in addition to the limited number of collected cloud-free imagery, LST changes were affected by cloud-induced noise from undetectable clouds, cloud shadows, and aerosols.

4.7.2. Future Directions

The findings of this study indicate that the majority of SUHI research has been concentrated in South Asian nations (Section 3.2), namely China and India, with less attention paid to cities in developing countries in other continents, particularly Africa and South America. Nine studies were interested in cities of six African countries—Cairo [5,106,113,143], Ethekwini [77], Hawassa [79], Akure [153], Osogbo [130], and Accra [170]. Only Brazilian cities, including Rio de Janeiro [8,169], Cuiaba-Varzea Grande [171], and Paço do Lumiar [172], were investigated in South America. More SUHI studies targeting cities in the African and South American continents are highly recommended.

There is no doubt that SUHIs are heavily impacted by the spatial and temporal dynamics of LULC. The increase witnessed in SUHI magnitude in several cities is attributed to IS horizontal expansion to the detriment of previous green and blue areas as a result of population growth and rising anthropogenic activities. As demonstrated in Section 4.5, however, other critical factors, such as seasonal variations, landscape composition and configuration, terrain characteristics in hilly and mountainous cities, and socioeconomic variables, highly contribute to the development of SUHIs. Nonetheless, it has been observed that only a few studies incorporated such important variables into their analyses. While acquiring data associated with some variables would be challenging in certain target areas, it is important to consider the changes of as many variables as possible while investigating SUHIs.

In the considered literature, most studies focused on exploring the past trends of SUHIs in regard to LULC changes. However, recent studies, although few (four publications),

have started to pay more attention to simulating future trends based on past ones. From this perspective, Tran et al. estimated future urban climate patterns based on predicted LULC changes in the Hanoi inner city [80]; the authors employed a nonparametric regression to predict future LST values in 2023 based on past LST spatial variations with respect to spatiotemporal changes witnessed within five LULC types (i.e., urban, vegetation, cropland, water, and bare land). The examined two scenarios regared whether future development growth would be low or high. From 2015 to 2023, the hotter LST zones (≥ 40 °C) were found to be likely to grow, while the cooler LST zones (≤ 38.5 °C) were found to tend to decline. From low-to-high growth scenarios, the same pattern was found to persist, albeit less pronounced. Guo et al. simulated two possible 2025 future scenarios in which LULC and LST in Beijing fluctuate depending on whether or not the city's population is controlled [59]. The authors used the conversion of land use and its effect at the small regional extent (CLUE-S) model to simulate LST based on land use demand that was estimated using a linear extrapolation of population and land use type. The population-controlled scenario had a projected reduction in future IS demand of 7.69%, resulting in a reduction of 1.1 °C in the average LST. Another investigation of the sort was reported by Wang et al. for the Chinese city of Nanjing [137], in which the authors simulated LULC patterns using the cellular automata-Markov chain model and estimated LST of the years 2030 and 2050 based on past trends (2000–2018); they subsequently defined areas of high and moderate risk depending on estimated LST values. The model predicted that high LST risk regions would increase, assuming urbanization is maintained from 2018 to 2050. A similar approach using the multilayer perceptron-Markov chain model was applied to Lahore city, Pakistan, to detect how future LULC changes would impact LST [173]. The findings suggested that if vegetation cover decreases by 3% in the next 15 years, there would be a rise of roughly 2 °C by 2035. The results of these studies are more relevant in the context that they provide concrete information to planners and decision-makers regarding future trends. Thus, future studies of this kind are strongly recommended.

5. Summary and Concluding Remarks

Since the turn of the century, research focused on historical and current SUHI trends with respect to LULC spatiotemporal changes in cities has significantly increased. This review shows that although case studies are growing, they have been geographically skewed. These studies have focused on South Asian cities, but other cities in emerging African or Latin American nations with fast urbanization trends have been less studied. Thus, more studies are highly required, especially in these cities, because gaining an accurate picture of SUHIs' long-term impacts is a crucial first step toward minimizing their consequences.

The increasing trend in SUHI studies is attributed to the free access to a multidecadal archive of satellite imagery data and the development of robust techniques for LULC extraction, LST retrieval, and the relationship assessment between the two. In terms of the used data, the Landsat series was the main source in most reviewed studies due to its long-term archived data dated back to the 1970s. On the other hand, MODIS and ASTER data were primarily used to assess SUHIs regarding day and night variations. Several methods to extract LULC from these datasets, notably the MLC, have been employed. In contrast to LULC extraction, LST retrieval is a complicated task due to the lack of a universal method that applies to all thermal sensors and the demanding nature of existing methods. Regression analysis was found to have been the most common way to evaluate LULC changes and LST.

SUHIs are strongly influenced by the spatial and temporal dynamics of LULC. The rise in SUHI magnitude seen in many cities is primarily linked to the horizontal expansion of ISs at the expense of formerly green and blue regions as a consequence of population growth and increased human activity. However, other important factors such as seasonal changes, landscape composition and configuration, topographical characteristics (especially in hilly

and mountainous cities), and socioeconomic determinants all play significant roles in the formation of SUHIs.

Specific mitigation measures to alleviate SUHIs are target area-specific, as they depend on geographical settings and climatic conditions. Nonetheless, four common strategies have been proposed in the revised literature: promoting greenery via planting and vertical greening, safeguarding waterbodies, utilizing solar-blocking materials for roofing and pavements, and adopting optimal urban designs.

The most significant limitation of SUHI studies concerns the inability to verify satellite-derived LSTs with in situ measurements from field surveys or historical data from climatological station networks. Another obstacle is related to the high cloud cover in remote sensing data, particularly in tropical cities. In addition, it was found that few papers included other critical factors (e.g., socioeconomic variables, topography, and landscape metrics) in their analysis to assess SUHI evolution.

In terms of prospects for SUHI research, the addition of other characteristics such as geography and socioeconomic variables will provide more insight into how SUHIs are evolving. This will enable the more realistic modeling of future SUHI trends based on historical patterns. The results of such research will be useful to planners and decision-makers because they will provide specific information regarding future trends.

Supplementary Materials: The following are available online at <https://www.mdpi.com/article/10.3390/rs13183654/s1>. Table S1: Descriptive list of the reviewed literature sorted chronologically based on year of publication (YoP).

Author Contributions: Conceptualization, A.D. and R.W.; methodology, A.D. and R.W.; writing—original draft preparation, A.D. and R.W.; writing—review and editing, A.D., R.W., Y.M. and T.O.; visualization, A.D. and R.W.; supervision, Y.M. and T.O.; funding acquisition, Y.M. All authors have read and agreed to the published version of the manuscript.

Funding: This research was partly supported by JSPS grant 21K01027.

Institutional Review Board Statement: Not applicable.

Informed Consent Statement: Not applicable.

Data Availability Statement: Not applicable.

Acknowledgments: The authors would like to thank the editors and the anonymous reviewers for their valuable comments that improved the final version of this article. The first author would also like to extend his gratitude to the Yoshida Scholarship Foundation for the funding received to undertake his PhD.

Conflicts of Interest: The authors declare no conflict of interest.

Appendix A

Table A1. Characteristics of the satellite data sources used in SUHI studies.

Thermal Sensors		MSS/TM/ETM+/TIRS	MODIS	ASTER
Carrier Satellite		Landsat Series	Aqua and Terra	Terra
Resolution	Spatial	30 m ¹	250 m (bands 1–2) 500 m (bands 3–7) 1000 m (bands 8–36)	VNIR: 15 m SWIR: 30 m TIR: 90 m
	Temporal	16 days	1–2 days	1–16 days
Coverage	Swath	L4: 170 × 183 km L5: Width (185 km) L7: Width (185 km) L8: 185 × 180 km	2330 × 10 km	60 × 60 km

Table A1. Cont.

Thermal Sensors	MSS/TM/ETM+/TIRS	MODIS	ASTER
Temporal	L4: 1982–2001 L5: 1984–2013 L7: 1999–ongoing L8: 2013–ongoing	Terra: since 1999 Aqua: since 2002	1999–ongoing (Terra)
Sensors	L4: MSS and TM L5: MSS and TM L7: ETM+ L8: OLI and TIRS	Terra MODIS (1999) Aqua MODIS (2002)	Terra ASTER (1999)

¹ The spatial resolution of thermal infrared band 6 of L4 is 120 m.

Table A2. List of the most common indices employed in the reviewed literature.

Index Category	Index	Name	Reference	Studies Share	
Vegetation	NDVI	Normalized Difference Vegetation Index	[174]	58.2%	
	FVC	Fractional Vegetation Cover	[175]	9.1%	
	SAVI	Soil-Adjusted Vegetation Index	[176]	2.7%	
	TDVI	Transformed Difference Vegetation Index	[177]	0.9%	
	EVI	Enhanced Vegetation Index	[178]	0.9%	
Biophysical	Built-Up	NDBI	Normalized Difference Built-Up Index	[179]	32.9%
		IBI	Index-Based Built-Up Index	[180]	1.2%
		EBBI	Enhanced Built-Up and Bareness Index	[181]	3.7%
		NDISI	Normalized Difference Impervious Surface Index	[182]	1.2%
		DBI	Dry Built-up Index	[183]	1.2%
Water	NDWI	Modified Difference Water Index	[184,185]	9.8%	
	MNDWI	Modified Normalized Difference Water Index	[186]	8.5%	
	LSWI	Land Surface Water Index	[187]	1.2%	
	NDMI	Normalized Difference Moisture Index	Used in [85,154]	1.2%	
Bare Land	NDBaI	Normalized Difference Bareness Index	[188]	7.3%	
	DBSI	Dry Bare-Soil Index	[183]	2.4%	
Landscape Composition	PLAND	Percentage of Landscape area			
	SHEI	Shannon's Evenness Index			
	SHDI	Shannon's Diversity Index			
Landscape Configuration	ED	Edge Density	[189]	8.5%	
	PD	Patch Density			
	LSI	Landscape Shape Index			
	CI	Clumpiness Index			
	CONTAG	Contagion			
COHESION	Patch Cohesion Index				

References

- Hobsbawm, E. *The Age of Revolution: 1789–1848*, 1st ed.; Vintage: New York, NY, USA, 1996; p. 27. ISBN 978-0-679-77253-8.
- Davis, K. The Origin and Growth of Urbanization in the World. *Am. J. Sociol.* **1955**, *60*, 429–437. [CrossRef]
- UNSD. *Demographic Yearbook 2019*; UNSD: New York, NY, USA, 2021; ISBN 978-92-1-148351-2.
- United Nations. *The World's Cities in 2018—Data Booklet*; United Nations: New York, NY, USA, 2018; ISBN 978-92-1-047610-2.
- Fan, C.; Myint, S.W.; Kaplan, S.; Middel, A.; Zheng, B.; Rahman, A.; Huang, H.-P.; Brazel, A.; Blumberg, D.G. Understanding the Impact of Urbanization on Surface Urban Heat Islands—A Longitudinal Analysis of the Oasis Effect in Subtropical Desert Cities. *Remote Sens.* **2017**, *9*, 672. [CrossRef]
- Oke, T.R. The Heat Island of the Urban Boundary Layer: Characteristics, Causes and Effects. In *Wind Climate in Cities*; Cermak, J.E., Davenport, A.G., Plate, E.J., Viegas, D.X., Eds.; NATO ASI Series; Springer: Dordrecht, The Netherlands, 1995; pp. 81–107, ISBN 978-94-017-3686-2.
- Manley, G. On the Frequency of Snowfall in Metropolitan England. *Q. J. R. Meteorol. Soc.* **1958**, *84*, 70–72. [CrossRef]
- Lucena, A.J.; Rotunno Filho, O.C.; França, J.R.A.; Peres, L.F.; Xavier, L.N.R. Urban Climate and Clues of Heat Island Events in the Metropolitan Area of Rio de Janeiro. *Theor. Appl. Climatol.* **2013**, *111*, 497–511. [CrossRef]
- Howard, L. *The Climate of London: Deduced from Meteorological Observations*, 1st ed.; Cambridge University Press: Cambridge, UK, 2012; ISBN 978-1-108-04951-1.
- Zhou, D.; Xiao, J.; Bonafoni, S.; Berger, C.; Deilami, K.; Zhou, Y.; Froking, S.; Yao, R.; Qiao, Z.; Sobrino, J.A. Satellite Remote Sensing of Surface Urban Heat Islands: Progress, Challenges, and Perspectives. *Remote Sens.* **2019**, *11*, 48. [CrossRef]

11. Kikon, N.; Singh, P.; Singh, S.K.; Vyas, A. Assessment of Urban Heat Islands (UHI) of Noida City, India Using Multi-Temporal Satellite Data. *Sustain. Cities Soc.* **2016**, *22*, 19–28. [[CrossRef](#)]
12. Estoque, R.C.; Murayama, Y. Monitoring Surface Urban Heat Island Formation in a Tropical Mountain City Using Landsat Data (1987–2015). *ISPRS J. Photogramm. Remote Sens.* **2017**, *133*, 18–29. [[CrossRef](#)]
13. Oke, T.R. The Energetic Basis of the Urban Heat Island. *Q. J. R. Meteorol. Soc.* **1982**, *108*, 1–24. [[CrossRef](#)]
14. Singh, P.; Kikon, N.; Verma, P. Impact of Land Use Change and Urbanization on Urban Heat Island in Lucknow City, Central India. A Remote Sensing Based Estimate. *Sustain. Cities Soc.* **2017**, *32*, 100–114. [[CrossRef](#)]
15. US EPA. Heat Island Impacts. Available online: <https://www.epa.gov/heatislands/heat-island-impacts> (accessed on 17 July 2021).
16. Gasparrini, A.; Guo, Y.; Hashizume, M.; Lavigne, E.; Zanobetti, A.; Schwartz, J.; Tobias, A.; Tong, S.; Rocklöv, J.; Forsberg, B.; et al. Mortality Risk Attributable to High and Low Ambient Temperature: A Multicountry Observational Study. *Lancet* **2015**, *386*, 369–375. [[CrossRef](#)]
17. Hsiang, S.; Kopp, R.; Jina, A.; Rising, J.; Delgado, M.; Mohan, S.; Rasmussen, D.J.; Muir-Wood, R.; Wilson, P.; Oppenheimer, M.; et al. Estimating Economic Damage from Climate Change in the United States. *Science* **2017**, *356*, 1362–1369. [[CrossRef](#)]
18. Ye, X.; Wolff, R.; Yu, W.; Vaneckova, P.; Pan, X.; Tong, S. Ambient Temperature and Morbidity: A Review of Epidemiological Evidence. *Environ. Health Perspect.* **2012**, *120*, 19–28. [[CrossRef](#)] [[PubMed](#)]
19. Vicedo-Cabrera, A.M.; Scovronick, N.; Sera, F.; Royé, D.; Schneider, R.; Tobias, A.; Astrom, C.; Guo, Y.; Honda, Y.; Hondula, D.M.; et al. The Burden of Heat-Related Mortality Attributable to Recent Human-Induced Climate Change. *Nat. Clim. Chang.* **2021**, *11*, 492–500. [[CrossRef](#)] [[PubMed](#)]
20. Wang, H.; Zhang, Y.; Tsou, J.Y.; Li, Y. Surface Urban Heat Island Analysis of Shanghai (China) Based on the Change of Land Use and Land Cover. *Sustainability* **2017**, *9*, 1538. [[CrossRef](#)]
21. Zhao, Y.; Xia, J.; Xu, Z.; Zou, L.; Qiao, Y.; Li, P. Impact of Urban Expansion on Rain Island Effect in Jinan City, North China. *Remote Sens.* **2021**, *13*, 2989. [[CrossRef](#)]
22. Sharma, R.; Joshi, P.K. Identifying Seasonal Heat Islands in Urban Settings of Delhi (India) Using Remotely Sensed Data—An Anomaly Based Approach. *Urban Clim.* **2014**, *9*, 19–34. [[CrossRef](#)]
23. Yuan, F.; Bauer, M.E. Comparison of Impervious Surface Area and Normalized Difference Vegetation Index as Indicators of Surface Urban Heat Island Effects in Landsat Imagery. *Remote Sens. Environ.* **2007**, *106*, 375–386. [[CrossRef](#)]
24. Imhoff, M.L.; Zhang, P.; Wolfe, R.E.; Bounoua, L. Remote Sensing of the Urban Heat Island Effect across Biomes in the Continental USA. *Remote Sens. Environ.* **2010**, *114*, 504–513. [[CrossRef](#)]
25. Papanastasiou, D.K.; Kittas, C. Maximum Urban Heat Island Intensity in a Medium-Sized Coastal Mediterranean City. *Theor. Appl. Climatol.* **2012**, *107*, 407–416. [[CrossRef](#)]
26. Grimmond, S. Urbanization and Global Environmental Change: Local Effects of Urban Warming. *Geogr. J.* **2007**, *173*, 83–88. [[CrossRef](#)]
27. Tran, H.; Uchihama, D.; Ochi, S.; Yasuoka, Y. Assessment with Satellite Data of the Urban Heat Island Effects in Asian Mega Cities. *Int. J. Appl. Earth Obs. Geoinf.* **2006**, *8*, 34–48. [[CrossRef](#)]
28. Voogt, J.A.; Oke, T.R. Thermal Remote Sensing of Urban Climates. *Remote Sens. Environ.* **2003**, *86*, 370–384. [[CrossRef](#)]
29. Roth, M.; Oke, T.R.; Emery, W.J. Satellite-Derived Urban Heat Islands from Three Coastal Cities and the Utilization of Such Data in Urban Climatology. *Int. J. Remote Sens.* **1989**, *10*, 1699–1720. [[CrossRef](#)]
30. Oke, T.R. The Distinction between Canopy and Boundary-layer Urban Heat Islands. *Atmosphere* **1976**, *14*, 268–277. [[CrossRef](#)]
31. Lo, C.P.; Quattrochi, D.A. Land-Use and Land-Cover Change, Urban Heat Island Phenomenon, and Health Implications: A Remote Sensing Approach. *Photogramm. Eng. Remote Sens.* **2003**, *69*, 1053–1063. [[CrossRef](#)]
32. Cermak, J.E.; Davenport, A.G.; Plate, E.J.; Viegas, D.X. *Wind Climate in Cities*; Springer Science & Business Media: Berlin/Heidelberg, Germany, 1994; ISBN 978-0-7923-3202-2.
33. Senanayake, I.P.; Welivitiya, W.D.D.P.; Nadeeka, P.M. Remote Sensing Based Analysis of Urban Heat Islands with Vegetation Cover in Colombo City, Sri Lanka Using Landsat-7 ETM+ Data. *Urban Clim.* **2013**, *5*, 19–35. [[CrossRef](#)]
34. Rao, P.K. Remote Sensing of Urban Heat Islands from an Environmental Satellite. *Bull. Am. Meteorol. Soc.* **1972**, *53*, 647–648.
35. Matson, M.; McClain, E.P.; McGinnis, D.F., Jr.; Pritchard, J.A. Satellite Detection of Urban Heat Islands. *Mon. Weather Rev.* **1978**, *106*, 1725–1734. [[CrossRef](#)]
36. Price, J.C. Assessment of the Urban Heat Island Effect through the Use of Satellite Data. *Mon. Weather Rev.* **1979**, *107*, 1554–1557. [[CrossRef](#)]
37. Mohamed, A.A.; Odindi, J.; Mutanga, O. Land Surface Temperature and Emissivity Estimation for Urban Heat Island Assessment Using Medium- and Low-Resolution Space-Borne Sensors: A Review. *Geocarto Int.* **2017**, *32*, 455–470. [[CrossRef](#)]
38. Deilami, K.; Kamruzzaman, M.; Liu, Y. Urban Heat Island Effect: A Systematic Review of Spatio-Temporal Factors, Data, Methods, and Mitigation Measures. *Int. J. Appl. Earth Obs. Geoinf.* **2018**, *67*, 30–42. [[CrossRef](#)]
39. Degirmenci, K.; Desouza, K.C.; Fieuw, W.; Watson, R.T.; Yigitcanlar, T. Understanding Policy and Technology Responses in Mitigating Urban Heat Islands: A Literature Review and Directions for Future Research. *Sustain. Cities Soc.* **2021**, *70*, 102873. [[CrossRef](#)]
40. Kotharkar, R.; Ramesh, A.; Bagade, A. Urban Heat Island Studies in South Asia: A Critical Review. *Urban Clim.* **2018**, *24*, 1011–1026. [[CrossRef](#)]

41. Sultana, S.; Satyanarayana, A.N.V. Urban Heat Island Intensity during Winter over Metropolitan Cities of India Using Remote-Sensing Techniques: Impact of Urbanization. *Int. J. Remote Sens.* **2018**, *39*, 6692–6730. [[CrossRef](#)]
42. Beck, H.E.; Zimmermann, N.E.; McVicar, T.R.; Vergopolan, N.; Berg, A.; Wood, E.F. Present and Future Köppen-Geiger Climate Classification Maps at 1-Km Resolution. *Sci. Data* **2018**, *5*, 180214. [[CrossRef](#)] [[PubMed](#)]
43. Simmons, M.T. Climates and Microclimates: Challenges for Extensive Green Roof Design in Hot Climates. In *Green Roof Ecosystems*; Sutton, R.K., Ed.; Ecological Studies; Springer International Publishing: Cham, Switzerland, 2015; pp. 63–80, ISBN 978-3-319-14983-7.
44. IMF. *World Economic Outlook (WEO)*; World Economic and Financial Surveys; International Monetary Fund: Washington, DC, USA, 2020; pp. 159–162.
45. Chen, L.; Jiang, R.; Xiang, W.-N. Surface Heat Island in Shanghai and Its Relationship with Urban Development from 1989 to 2013. *Adv. Meteorol.* **2016**, *2016*, 9782686. [[CrossRef](#)]
46. Cui, L.; Shi, J. Urbanization and Its Environmental Effects in Shanghai, China. *Urban Clim.* **2012**, *2*, 1–15. [[CrossRef](#)]
47. Du, H.; Zhou, F.; Li, C.; Cai, W.; Jiang, H.; Cai, Y. Analysis of the Impact of Land Use on Spatiotemporal Patterns of Surface Urban Heat Island in Rapid Urbanization, a Case Study of Shanghai, China. *Sustainability* **2020**, *12*, 1171. [[CrossRef](#)]
48. Hu, Y.; Hou, M.; Jia, G.; Zhao, C.; Zhen, X.; Xu, Y. Comparison of Surface and Canopy Urban Heat Islands within Megacities of Eastern China. *ISPRS J. Photogramm. Remote Sens.* **2019**, *156*, 160–168. [[CrossRef](#)]
49. Li, J.-J.; Wang, X.-R.; Wang, X.-J.; Ma, W.-C.; Zhang, H. Remote Sensing Evaluation of Urban Heat Island and Its Spatial Pattern of the Shanghai Metropolitan Area, China. *Ecol. Complex.* **2009**, *6*, 413–420. [[CrossRef](#)]
50. Li, J.; Song, C.; Cao, L.; Zhu, F.; Meng, X.; Wu, J. Impacts of Landscape Structure on Surface Urban Heat Islands: A Case Study of Shanghai, China. *Remote Sens. Environ.* **2011**, *115*, 3249–3263. [[CrossRef](#)]
51. Li, Y.-Y.; Zhang, H.; Kainz, W. Monitoring Patterns of Urban Heat Islands of the Fast-Growing Shanghai Metropolis, China: Using Time-Series of Landsat TM/ETM+ Data. *Int. J. Appl. Earth Obs. Geoinf.* **2012**, *19*, 127–138. [[CrossRef](#)]
52. Zhang, H.; Qi, Z.-F.; Ye, X.-Y.; Cai, Y.-B.; Ma, W.-C.; Chen, M.-N. Analysis of Land Use/Land Cover Change, Population Shift, and Their Effects on Spatiotemporal Patterns of Urban Heat Islands in Metropolitan Shanghai, China. *Appl. Geogr.* **2013**, *44*, 121–133. [[CrossRef](#)]
53. Kant, Y.; Bharath, B.D.; Mallick, J.; Atzberger, C.; Kerle, N. Satellite-Based Analysis of the Role of Land Use/Land Cover and Vegetation Density on Surface Temperature Regime of Delhi, India. *J. Indian Soc. Remote Sens.* **2009**, *37*, 201–214. [[CrossRef](#)]
54. Mallick, J.; Rahman, A.; Singh, C.K. Modeling Urban Heat Islands in Heterogeneous Land Surface and Its Correlation with Impervious Surface Area by Using Night-Time ASTER Satellite Data in Highly Urbanizing City, Delhi-India. *Adv. Space Res.* **2013**, *52*, 639–655. [[CrossRef](#)]
55. Pramanik, S.; Punia, M. Land Use/Land Cover Change and Surface Urban Heat Island Intensity: Source—Sink Landscape-Based Study in Delhi, India. *Environ. Dev. Sustain.* **2020**, *22*, 7331–7356. [[CrossRef](#)]
56. Singh, R.B.; Grover, A.; Zhan, J. Inter-Seasonal Variations of Surface Temperature in the Urbanized Environment of Delhi Using Landsat Thermal Data. *Energies* **2014**, *7*, 1811–1828. [[CrossRef](#)]
57. Cai, G.; Du, M.; Xue, Y. Monitoring of Urban Heat Island Effect in Beijing Combining ASTER and TM Data. *Int. J. Remote Sens.* **2011**, *32*, 1213–1232. [[CrossRef](#)]
58. Ding, H.; Shi, W. Land-Use/Land-Cover Change and Its Influence on Surface Temperature: A Case Study in Beijing City. *Int. J. Remote Sens.* **2013**, *34*, 5503–5517. [[CrossRef](#)]
59. Guo, L.; Liu, R.; Men, C.; Wang, Q.; Miao, Y.; Zhang, Y. Quantifying and Simulating Landscape Composition and Pattern Impacts on Land Surface Temperature: A Decadal Study of the Rapidly Urbanizing City of Beijing, China. *Sci. Total Environ.* **2019**, *654*, 430–440. [[CrossRef](#)]
60. Ye, C.; Chen, R.; Li, Y.; Liu, T.; Diao, K.; Li, J. Characterization of Combined Effects of Urban Built-Up and Vegetated Areas on Long-Term Urban Heat Islands in Beijing. *Can. J. Remote Sens.* **2019**, *45*, 634–649. [[CrossRef](#)]
61. Kamruzzaman, M.; Deilami, K.; Yigitcanlar, T. Investigating the Urban Heat Island Effect of Transit Oriented Development in Brisbane. *J. Transp. Geogr.* **2018**, *66*, 116–124. [[CrossRef](#)]
62. Bokaie, M.; Shamsipour, A.; Khatibi, P.; Hosseini, A. Seasonal Monitoring of Urban Heat Island Using Multi-Temporal Landsat and MODIS Images in Tehran. *Int. J. Urban Sci.* **2019**, *23*, 269–285. [[CrossRef](#)]
63. Xiong, Y.; Huang, S.; Chen, F.; Ye, H.; Wang, C.; Zhu, C. The Impacts of Rapid Urbanization on the Thermal Environment: A Remote Sensing Study of Guangzhou, South China. *Remote Sens.* **2012**, *4*, 2033–2056. [[CrossRef](#)]
64. Padmanaban, R.; Bhowmik, A.K.; Cabral, P. Satellite Image Fusion to Detect Changing Surface Permeability and Emerging Urban Heat Islands in a Fast-Growing City. *PLoS ONE* **2019**, *14*, e0208949. [[CrossRef](#)]
65. Dhar, R.B.; Chakraborty, S.; Chattopadhyay, R.; Sikdar, P.K. Impact of Land-Use/Land-Cover Change on Land Surface Temperature Using Satellite Data: A Case Study of Rajarhat Block, North 24-Parganas District, West Bengal. *J. Indian Soc. Remote Sens.* **2019**, *47*, 331–348. [[CrossRef](#)]
66. Wulder, M.A.; Masek, J.G.; Cohen, W.B.; Loveland, T.R.; Woodcock, C.E. Opening the Archive: How Free Data Has Enabled the Science and Monitoring Promise of Landsat. *Remote Sens. Environ.* **2012**, *122*, 2–10. [[CrossRef](#)]
67. Melaas, E.K.; Wang, J.A.; Miller, D.L.; Friedl, M.A. Interactions between Urban Vegetation and Surface Urban Heat Islands: A Case Study in the Boston Metropolitan Region. *Environ. Res. Lett.* **2016**, *11*, 054020. [[CrossRef](#)]

68. Zhang, W.; Liu, S. Applications of the Small Satellite Constellation for Environment and Disaster Monitoring and Forecasting. *Int. J. Disaster Risk Sci.* **2010**, *1*, 9–16. [CrossRef]
69. Wang, Q.; Wu, C.Q.; Li, Q.; Li, J.S. Chinese HJ-1A/B Satellites and Data Characteristics. *Sci. China Earth Sci.* **2010**, *53*, 51–57. [CrossRef]
70. Wu, H.; Ye, L.-P.; Shi, W.-Z.; Clarke, K.C. Assessing the Effects of Land Use Spatial Structure on Urban Heat Islands Using HJ-1B Remote Sensing Imagery in Wuhan, China. *Int. J. Appl. Earth Obs. Geoinf.* **2014**, *32*, 67–78. [CrossRef]
71. Rasul, A.; Balzter, H.; Smith, C. Spatial Variation of the Daytime Surface Urban Cool Island during the Dry Season in Erbil, Iraqi Kurdistan, from Landsat 8. *Urban Clim.* **2015**, *14*, 176–186. [CrossRef]
72. Cai, Y.; Zhang, H.; Zheng, P.; Pan, W. Quantifying the Impact of Land Use/Land Cover Changes on the Urban Heat Island: A Case Study of the Natural Wetlands Distribution Area of Fuzhou City, China. *Wetlands* **2016**, *36*, 285–298. [CrossRef]
73. Min, M.; Zhao, H.; Miao, C. Spatio-Temporal Evolution Analysis of the Urban Heat Island: A Case Study of Zhengzhou City, China. *Sustainability* **2018**, *10*, 1992. [CrossRef]
74. Majkowska, A.; Kolendowicz, L.; Pórolniczak, M.; Hauke, J.; Czernecki, B. The Urban Heat Island in the City of Poznań as Derived from Landsat 5 TM. *Theor. Appl. Climatol.* **2017**, *128*, 769–783. [CrossRef]
75. Land Monitoring Service. CORINE Land Cover—Copernicus Land Monitoring Service. Available online: <https://land.copernicus.eu/pan-european/corine-land-cover> (accessed on 18 July 2021).
76. Dihkan, M.; Karli, F.; Guneroglu, N.; Guneroglu, A. Evaluation of Urban Heat Island Effect in Turkey. *Arab. J. Geosci.* **2018**, *11*, 186. [CrossRef]
77. Odindi, J.O.; Bangamwabo, V.; Mutanga, O. Assessing the Value of Urban Green Spaces in Mitigating Multi-Seasonal Urban Heat Using MODIS Land Surface Temperature (LST) and Landsat 8 Data. *Int. J. Environ. Res.* **2015**, *9*, 9–18.
78. Huang, X.; Wang, Y. Investigating the Effects of 3D Urban Morphology on the Surface Urban Heat Island Effect in Urban Functional Zones by Using High-Resolution Remote Sensing Data: A Case Study of Wuhan, Central China. *ISPRS J. Photogramm. Remote Sens.* **2019**, *152*, 119–131. [CrossRef]
79. Chaka, D.S.; Oda, T.K. Understanding Land Surface Temperature on Rift Areas to Examine the Spatial Variation of Urban Heat Island: The Case of Hawassa, Southern Ethiopia. *GeoJournal* **2019**, *86*, 993–1014. [CrossRef]
80. Tran, D.X.; Pla, F.; Latorre-Carmona, P.; Myint, S.W.; Caetano, M.; Kieu, H.V. Characterizing the Relationship between Land Use Land Cover Change and Land Surface Temperature. *ISPRS J. Photogramm. Remote Sens.* **2017**, *124*, 119–132. [CrossRef]
81. Dissanayake, D.M.S.L.B.; Morimoto, T.; Ranagalage, M.; Murayama, Y. Land-Use/Land-Cover Changes and Their Impact on Surface Urban Heat Islands: Case Study of Kandy City, Sri Lanka. *Climate* **2019**, *7*, 99. [CrossRef]
82. Priyankara, P.; Ranagalage, M.; Dissanayake, D.M.S.L.B.; Morimoto, T.; Murayama, Y. Spatial Process of Surface Urban Heat Island in Rapidly Growing Seoul Metropolitan Area for Sustainable Urban Planning Using Landsat Data (1996–2017). *Climate* **2019**, *7*, 110. [CrossRef]
83. Ranagalage, M.; Dmslb, D.; Murayama, Y.; Zhang, X.; Estoque, R.C.; Enc, P.; Morimoto, T. Quantifying Surface Urban Heat Island Formation in the World Heritage Tropical Mountain City of Sri Lanka. *ISPRS Int. J. Geo-Inf.* **2018**, *7*, 341. [CrossRef]
84. Khan, M.S.; Ullah, S.; Sun, T.; Rehman, A.U.; Chen, L. Land-Use/Land-Cover Changes and Its Contribution to Urban Heat Island: A Case Study of Islamabad, Pakistan. *Sustainability* **2020**, *12*, 3861. [CrossRef]
85. Roy, S.; Pandit, S.; Eva, E.A.; Bagmar, M.S.H.; Papia, M.; Banik, L.; Dube, T.; Rahman, F.; Razi, M.A. Examining the Nexus between Land Surface Temperature and Urban Growth in Chattogram Metropolitan Area of Bangladesh Using Long Term Landsat Series Data. *Urban Clim.* **2020**, *32*. [CrossRef]
86. Atasoy, M. Assessing the Impacts of Land-Use/Land-Cover Change on the Development of Urban Heat Island Effects. *Environ. Dev. Sustain.* **2020**, *22*, 7547–7557. [CrossRef]
87. Chen, X.-L.; Zhao, H.-M.; Li, P.-X.; Yin, Z.-Y. Remote Sensing Image-Based Analysis of the Relationship between Urban Heat Island and Land Use/Cover Changes. *Remote Sens. Environ.* **2006**, *104*, 133–146. [CrossRef]
88. Choudhury, D.; Das, K.; Das, A. Assessment of Land Use Land Cover Changes and Its Impact on Variations of Land Surface Temperature in Asansol-Durgapur Development Region. *Egypt. J. Remote Sens. Space Sci.* **2019**, *22*, 203–218. [CrossRef]
89. Ghosh, S.; Chatterjee, N.D.; Dinda, S. Relation between Urban Biophysical Composition and Dynamics of Land Surface Temperature in the Kolkata Metropolitan Area: A GIS and Statistical Based Analysis for Sustainable Planning. *Modeling Earth Syst. Environ.* **2019**, *5*, 307–329. [CrossRef]
90. Grigoraş, G.; Urişescu, B. Land Use/Land Cover Changes Dynamics and Their Effects on Surface Urban Heat Island in Bucharest, Romania. *Int. J. Appl. Earth Obs. Geoinf.* **2019**, *80*, 115–126. [CrossRef]
91. Gupta, N.; Mathew, A.; Khandelwal, S. Spatio-Temporal Impact Assessment of Land Use / Land Cover (LU-LC) Change on Land Surface Temperatures over Jaipur City in India. *Int. J. Urban Sustain. Dev.* **2020**. [CrossRef]
92. Hoan, N.T.; Liou, Y.-A.; Nguyen, K.-A.; Sharma, R.C.; Tran, D.-P.; Liou, C.-L.; Cham, D.D. Assessing the Effects of Land-Use Types in Surface Urban Heat Islands for Developing Comfortable Living in Hanoi City. *Remote Sens.* **2018**, *10*, 1965. [CrossRef]
93. Lakra, K.; Sharma, D. Geospatial Assessment of Urban Growth Dynamics and Land Surface Temperature in Ajmer Region, India. *J. Indian Soc. Remote Sens.* **2019**, *47*, 1073–1089. [CrossRef]
94. Lu, D.; Song, K.; Zang, S.; Jia, M.; Du, J.; Ren, C. The Effect of Urban Expansion on Urban Surface Temperature in Shenyang, China: An Analysis with Landsat Imagery. *Environ. Model. Assess.* **2015**, *20*, 197–210. [CrossRef]

95. Miky, Y.H. Remote Sensing Analysis for Surface Urban Heat Island Detection over Jeddah, Saudi Arabia. *Appl. Geomat.* **2019**, *11*, 243–258. [[CrossRef](#)]
96. Nguyen, T.M.; Lin, T.-H.; Chan, H.-P. The Environmental Effects of Urban Development in Hanoi, Vietnam from Satellite and Meteorological Observations from 1999–2016. *Sustainability* **2019**, *11*, 1768. [[CrossRef](#)]
97. Pal, S.; Ziaul, S. Detection of Land Use and Land Cover Change and Land Surface Temperature in English Bazar Urban Centre. *Egypt. J. Remote Sens. Space Sci.* **2017**, *20*, 125–145. [[CrossRef](#)]
98. Rousta, I.; Sarif, M.O.; Gupta, R.D.; Olafsson, H.; Ranagalage, M.; Murayama, Y.; Zhang, H.; Mushore, T.D. Spatiotemporal Analysis of Land Use/Land Cover and Its Effects on Surface Urban Heat Island Using Landsat Data: A Case Study of Metropolitan City Tehran (1988–2018). *Sustainability* **2018**, *10*, 4433. [[CrossRef](#)]
99. Wang, C.; Myint, S.W.; Wang, Z.; Song, J. Spatio-Temporal Modeling of the Urban Heat Island in the Phoenix Metropolitan Area: Land Use Change Implications. *Remote Sens.* **2016**, *8*, 185. [[CrossRef](#)]
100. Cohen, J. A Coefficient of Agreement for Nominal Scales. *Educ. Psychol. Meas.* **1960**, *20*, 37–46. [[CrossRef](#)]
101. Monserud, R.A.; Leemans, R. Comparing Global Vegetation Maps with the Kappa Statistic. *Ecol. Model.* **1992**, *62*, 275–293. [[CrossRef](#)]
102. Anderson, J.R.; Hardy, E.E.; Roach, J.T.; Witmer, R.E. *A Land Use and Land Cover Classification System for Use with Remote Sensor Data*; Professional Paper; U.S. Government Printing Office: Washington, DC, USA, 1976; Volume 964.
103. Townshend, J.R. *Terrain Analysis and Remote Sensing*, 1st ed.; Unwin Hyman: London, UK, 1981; ISBN 978-0-04-551037-5.
104. Lea, C.; Curtis, A.C. *Thematic Accuracy Assessment Procedures: National Park Service Vegetation Inventory*; Natural Resource Report; Version 2.0.; U.S. Department of the Interior, National Park Service, Natural Resource Program Center: Fort Collins, CO, USA, 2010.
105. Lillesand, T.; Kiefer, R.W.; Chipman, J. *Remote Sensing and Image Interpretation*; John Wiley & Sons: Hoboken, NJ, USA, 2015; ISBN 978-1-118-34328-9.
106. Hereher, M.E. Retrieving Spatial Variations of Land Surface Temperatures from Satellite Data—Cairo Region, Egypt. *Geocarto Int.* **2017**, *32*, 556–568. [[CrossRef](#)]
107. Meng, F.; Liu, M. Remote-Sensing Image-Based Analysis of the Patterns of Urban Heat Islands in Rapidly Urbanizing Jinan, China. *Int. J. Remote Sens.* **2013**, *34*, 8838–8853. [[CrossRef](#)]
108. Zhou, X.; Wang, Y.-C. Dynamics of Land Surface Temperature in Response to Land-Use/Cover Change. *Geogr. Res.* **2011**, *49*, 23–36. [[CrossRef](#)]
109. Zhang, Y.; Odeh, I.O.A.; Han, C. Bi-Temporal Characterization of Land Surface Temperature in Relation to Impervious Surface Area, NDVI and NDBI, Using a Sub-Pixel Image Analysis. *Int. J. Appl. Earth Obs. Geoinf.* **2009**, *11*, 256–264. [[CrossRef](#)]
110. Yu, Z.; Guo, X.; Zeng, Y.; Koga, M.; Vejre, H. Variations in Land Surface Temperature and Cooling Efficiency of Green Space in Rapid Urbanization: The Case of Fuzhou City, China. *Urban For. Urban Green.* **2018**, *29*, 113–121. [[CrossRef](#)]
111. Zhang, X.; Wang, D.; Hao, H.; Zhang, F.; Hu, Y. Effects of Land Use/Cover Changes and Urban Forest Configuration on Urban Heat Islands in a Loess Hilly Region: Case Study Based on Yan’an City, China. *Int. J. Environ. Res. Public Health* **2017**, *14*, 840. [[CrossRef](#)]
112. Yang, C.; He, X.; Yan, F.; Yu, L.; Bu, K.; Yang, J.; Chang, L.; Zhang, S. Mapping the Influence of Land Use/Land Cover Changes on the Urban Heat Island Effect—A Case Study of Changchun, China. *Sustainability* **2017**, *9*, 312. [[CrossRef](#)]
113. Effat, H.A.; Hassan, O.A.K. Change Detection of Urban Heat Islands and Some Related Parameters Using Multi-Temporal Landsat Images; a Case Study for Cairo City, Egypt. *Urban Clim.* **2014**, *10*, 171–188. [[CrossRef](#)]
114. Yusuf, Y.A.; Pradhan, B.; Idrees, M.O. Spatio-Temporal Assessment of Urban Heat Island Effects in Kuala Lumpur Metropolitan City Using Landsat Images. *J. Indian Soc. Remote Sens.* **2014**, *42*, 829–837. [[CrossRef](#)]
115. Zhang, X.; Estoque, R.C.; Murayama, Y. An Urban Heat Island Study in Nanchang City, China Based on Land Surface Temperature and Social-Ecological Variables. *Sustain. Cities Soc.* **2017**, *32*, 557–568. [[CrossRef](#)]
116. Li, Z.-L.; Tang, B.-H.; Wu, H.; Ren, H.; Yan, G.; Wan, Z.; Trigo, I.F.; Sobrino, J.A. Satellite-Derived Land Surface Temperature: Current Status and Perspectives. *Remote Sens. Environ.* **2013**, *131*, 14–37. [[CrossRef](#)]
117. Khan, A.; Chatterjee, S.; Weng, Y. 2 - Characterizing thermal fields and evaluating UHI effects. In *Urban Heat Island Modeling for Tropical Climates*; Khan, A., Chatterjee, S., Weng, Y., Eds.; Elsevier: Amsterdam, The Netherlands, 2021; pp. 37–67, ISBN 978-0-12-819669-4.
118. Götsche, F.-M.; Olesen, F.-S.; Bork-Unkelbach, A. Validation of Land Surface Temperature Derived from MSG/SEVIRI with in Situ Measurements at Gobabeb, Namibia. *Int. J. Remote Sens.* **2013**, *34*, 3069–3083. [[CrossRef](#)]
119. Martin, M.A.; Ghent, D.; Pires, A.C.; Götsche, F.-M.; Cermak, J.; Remedios, J.J. Comprehensive In Situ Validation of Five Satellite Land Surface Temperature Data Sets over Multiple Stations and Years. *Remote Sens.* **2019**, *11*, 479. [[CrossRef](#)]
120. Srivastava, P.K.; Majumdar, T.J.; Bhattacharya, A.K. Surface Temperature Estimation in Singhbhum Shear Zone of India Using Landsat-7 ETM+ Thermal Infrared Data. *Adv. Space Res.* **2009**, *43*, 1563–1574. [[CrossRef](#)]
121. Feng, H.; Zhao, X.; Chen, F.; Wu, L. Using Land Use Change Trajectories to Quantify the Effects of Urbanization on Urban Heat Island. *Adv. Space Res.* **2014**, *53*, 463–473. [[CrossRef](#)]
122. Anding, D.; Kauth, R. Estimation of Sea Surface Temperature from Space. *Remote Sens. Environ.* **1970**, *1*, 217–220. [[CrossRef](#)]
123. Price, J.C. Estimating Surface Temperatures from Satellite Thermal Infrared Data—A Simple Formulation for the Atmospheric Effect. *Remote Sens. Environ.* **1983**, *13*, 353–361. [[CrossRef](#)]

124. Price, J.C. Land Surface Temperature Measurements from the Split Window Channels of the NOAA 7 Advanced Very High Resolution Radiometer. *J. Geophys. Res. Atmos.* **1984**, *89*, 7231–7237. [[CrossRef](#)]
125. Qin, Z.; Karnieli, A.; Berliner, P. A Mono-Window Algorithm for Retrieving Land Surface Temperature from Landsat TM Data and Its Application to the Israel-Egypt Border Region. *Int. J. Remote Sens.* **2001**, *22*, 3719–3746. [[CrossRef](#)]
126. Guha, S.; Govil, H.; Mukherjee, S. Dynamic Analysis and Ecological Evaluation of Urban Heat Islands in Raipur City, India. *J. Appl. Remote Sens.* **2017**, *11*, 036020. [[CrossRef](#)]
127. Saha, P.; Bandopadhyay, S.; Kumar, C.; Mitra, C. Multi-Approach Synergic Investigation between Land Surface Temperature and Land-Use Land-Cover. *J. Earth Syst. Sci.* **2020**, *129*, 74. [[CrossRef](#)]
128. Jiménez-Muñoz, J.C.; Sobrino, J.A. A Generalized Single-Channel Method for Retrieving Land Surface Temperature from Remote Sensing Data. *J. Geophys. Res. Atmos.* **2003**, *108*. [[CrossRef](#)]
129. Li, L.; Tan, Y.; Ying, S.; Yu, Z.; Li, Z.; Lan, H. Impact of Land Cover and Population Density on Land Surface Temperature: Case Study in Wuhan, China. *J. Appl. Remote Sens.* **2014**, *8*, 084993. [[CrossRef](#)]
130. Eresanya, E.O.; Daramola, M.T.; Durowoju, O.S.; Awoyele, P. Investigation of the Changing Patterns of the Land Use Land Cover over Osogbo and Its Environs. *R. Soc. Open Sci.* **2019**, *6*, 191021. [[CrossRef](#)]
131. Rizvi, S.H.; Fatima, H.; Iqbal, M.J.; Alam, K. The Effect of Urbanization on the Intensification of SUHIs: Analysis by LULC on Karachi. *J. Atmos. Sol. Terr. Phys.* **2020**, *207*, 105374. [[CrossRef](#)]
132. Oke, T.R. Towards Better Scientific Communication in Urban Climate. *Theor. Appl. Climatol.* **2006**, *84*, 179–190. [[CrossRef](#)]
133. Deilami, K.; Kamruzzaman, M.; Hayes, J.F. Correlation or Causality between Land Cover Patterns and the Urban Heat Island Effect? Evidence from Brisbane, Australia. *Remote Sens.* **2016**, *8*, 716. [[CrossRef](#)]
134. Siqi, J.; Yuhong, W. Effects of Land Use and Land Cover Pattern on Urban Temperature Variations: A Case Study in Hong Kong. *Urban Clim.* **2020**, *34*, 100693. [[CrossRef](#)]
135. Chakraborti, S.; Banerjee, A.; Sannigrahi, S.; Pramanik, S.; Maiti, A.; Jha, S. Assessing the Dynamic Relationship among Land Use Pattern and Land Surface Temperature: A Spatial Regression Approach. *Asian Geogr.* **2019**, *36*, 93–116. [[CrossRef](#)]
136. Kamali Maskooni, E.; Hashemi, H.; Berndtsson, R.; Daneshkar Arasteh, P.; Kazemi, M. Impact of Spatiotemporal Land-Use and Land-Cover Changes on Surface Urban Heat Islands in a Semiarid Region Using Landsat Data. *Int. J. Digit. Earth* **2021**, *14*, 250–270. [[CrossRef](#)]
137. Wang, R.; Hou, H.; Murayama, Y.; Derdouri, A. Spatiotemporal Analysis of Land Use/Cover Patterns and Their Relationship with Land Surface Temperature in Nanjing, China. *Remote Sens.* **2020**, *12*, 440. [[CrossRef](#)]
138. Dutta, I.; Das, A. Exploring the Spatio-Temporal Pattern of Regional Heat Island (RHI) in an Urban Agglomeration of Secondary Cities in Eastern India. *Urban Clim.* **2020**, *34*, 100679. [[CrossRef](#)]
139. Huang, Q.; Huang, J.; Yang, X.; Fang, C.; Liang, Y. Quantifying the Seasonal Contribution of Coupling Urban Land Use Types on Urban Heat Island Using Land Contribution Index: A Case Study in Wuhan, China. *Sustain. Cities Soc.* **2019**, *44*, 666–675. [[CrossRef](#)]
140. Xiong, Y.; Peng, F.; Zou, B. Spatiotemporal Influences of Land Use/Cover Changes on the Heat Island Effect in Rapid Urbanization Area. *Front. Earth Sci.* **2019**, *13*, 614–627. [[CrossRef](#)]
141. Amiri, R.; Weng, Q.; Alimohammadi, A.; Alavipanah, S.K. Spatial-Temporal Dynamics of Land Surface Temperature in Relation to Fractional Vegetation Cover and Land Use/Cover in the Tabriz Urban Area, Iran. *Remote Sens. Environ.* **2009**, *113*, 2606–2617. [[CrossRef](#)]
142. Amanollahi, J.; Tzani, C.; Ramli, M.F.; Abdullah, A.M. Urban Heat Evolution in a Tropical Area Utilizing Landsat Imagery. *Atmos. Res.* **2016**, *167*, 175–182. [[CrossRef](#)]
143. El-Hattab, M.; Amany, S.M.; Lamia, G.E. Monitoring and Assessment of Urban Heat Islands over the Southern Region of Cairo Governorate, Egypt. *Egypt. J. Remote Sens. Space Sci.* **2018**, *21*, 311–323. [[CrossRef](#)]
144. Hu, Y.; Jia, G. Influence of Land Use Change on Urban Heat Island Derived from Multi-Sensor Data. *Int. J. Climatol.* **2010**, *30*, 1382–1395. [[CrossRef](#)]
145. Ranagalage, M.; Estoque, R.C.; Murayama, Y. An Urban Heat Island Study of the Colombo Metropolitan Area, Sri Lanka, Based on Landsat Data (1997–2017). *ISPRS Int. J. Geo Inf.* **2017**, *6*, 189. [[CrossRef](#)]
146. Rani, M.; Kumar, P.; Pandey, P.C.; Srivastava, P.K.; Chaudhary, B.S.; Tomar, V.; Mandal, V.P. Multi-Temporal NDVI and Surface Temperature Analysis for Urban Heat Island Inbuilt Surrounding of Sub-Humid Region: A Case Study of Two Geographical Regions. *Remote Sens. Appl. Soc. Environ.* **2018**, *10*, 163–172. [[CrossRef](#)]
147. Saleem, M.S.; Ahmad, S.R.; Shafiq-Ur-Rehman; Javed, M. A. Impact Assessment of Urban Development Patterns on Land Surface Temperature by Using Remote Sensing Techniques: A Case Study of Lahore, Faisalabad and Multan District. *Environ. Sci. Pollut. Res.* **2020**, *27*, 39865–39878. [[CrossRef](#)]
148. Sannigrahi, S.; Rahmat, S.; Chakraborti, S.; Bhatt, S.; Jha, S. Changing Dynamics of Urban Biophysical Composition and Its Impact on Urban Heat Island Intensity and Thermal Characteristics: The Case of Hyderabad City, India. *Model. Earth Syst. Environ.* **2017**, *3*, 647–667. [[CrossRef](#)]
149. Sultana, S.; Satyanarayana, A.N.V. Assessment of Urbanisation and Urban Heat Island Intensities Using Landsat Imageries during 2000–2018 over a Sub-Tropical Indian City. *Sustain. Cities Soc.* **2020**, *52*, 101846. [[CrossRef](#)]
150. Rotem-Mindali, O.; Michael, Y.; Helman, D.; Lensky, I.M. The Role of Local Land-Use on the Urban Heat Island Effect of Tel Aviv as Assessed from Satellite Remote Sensing. *Appl. Geogr.* **2015**, *56*, 145–153. [[CrossRef](#)]

151. Karakuş, C.B. The Impact of Land Use/Land Cover (LULC) Changes on Land Surface Temperature in Sivas City Center and Its Surroundings and Assessment of Urban Heat Island. *Asia Pac. J. Atmos. Sci.* **2019**, *55*, 669–684. [[CrossRef](#)]
152. Lin, Y.; Jim, C.Y.; Deng, J.; Wang, Z. Urbanization Effect on Spatiotemporal Thermal Patterns and Changes in Hangzhou (China). *Build. Environ.* **2018**, *145*, 166–176. [[CrossRef](#)]
153. Makinde, E.O.; Agbor, C.F. Geoinformatic Assessment of Urban Heat Island and Land Use/Cover Processes: A Case Study from Akure. *Environ. Earth Sci.* **2019**, *78*, 483. [[CrossRef](#)]
154. Sahana, M.; Dutta, S.; Sajjad, H. Assessing Land Transformation and Its Relation with Land Surface Temperature in Mumbai City, India Using Geospatial Techniques. *Int. J. Urban Sci.* **2019**, *23*, 205–225. [[CrossRef](#)]
155. Song, Y.; Song, X.; Shao, G. Effects of Green Space Patterns on Urban Thermal Environment at Multiple Spatial-Temporal Scales. *Sustainability* **2020**, *12*, 6850. [[CrossRef](#)]
156. Turner, M.G. Landscape Ecology: What Is the State of the Science? *Annu. Rev. Ecol. Evol. Syst.* **2005**, *36*, 319–344. [[CrossRef](#)]
157. Dobrovolný, P. The Surface Urban Heat Island in the City of Brno (Czech Republic) Derived from Land Surface Temperatures and Selected Reasons for Its Spatial Variability. *Theor. Appl. Climatol.* **2013**, *112*, 89–98. [[CrossRef](#)]
158. Li, Y.-Y.; Liu, Y.; Ranagalage, M.; Zhang, H.; Zhou, R. Examining Land Use/Land Cover Change and the Summertime Surface Urban Heat Island Effect in Fast-Growing Greater Hefei, China: Implications for Sustainable Land Development. *ISPRS Int. J. Geo Inf.* **2020**, *9*, 568. [[CrossRef](#)]
159. Chen, Z.; Gong, C.; Wu, J.; Yu, S. The Influence of Socioeconomic and Topographic Factors on Nocturnal Urban Heat Islands: A Case Study in Shenzhen, China. *Int. J. Remote Sens.* **2012**, *33*, 3834–3849. [[CrossRef](#)]
160. Kleerekoper, L.; van Esch, M.; Salcedo, T.B. How to Make a City Climate-Proof, Addressing the Urban Heat Island Effect. *Resour. Conserv. Recycl.* **2012**, *64*, 30–38. [[CrossRef](#)]
161. Wong, N.H.; Tan, C.L.; Kolokotsa, D.D.; Takebayashi, H. Greenery as a Mitigation and Adaptation Strategy to Urban Heat. *Nat. Rev. Earth Environ.* **2021**, *2*, 166–181. [[CrossRef](#)]
162. Zhang, R. Cooling Effect and Control Factors of Common Shrubs on the Urban Heat Island Effect in a Southern City in China. *Sci. Rep.* **2020**, *10*, 17317. [[CrossRef](#)]
163. Zhou, G.; Wang, H.; Chen, W.; Zhang, G.; Luo, Q.; Jia, B. Impacts of Urban Land Surface Temperature on Tract Landscape Pattern, Physical and Social Variables. *Int. J. Remote Sens.* **2020**, *41*, 683–703. [[CrossRef](#)]
164. Ghosh, S.; Das, A. Modelling Urban Cooling Island Impact of Green Space and Water Bodies on Surface Urban Heat Island in a Continuously Developing Urban Area. *Model. Earth Syst. Environ.* **2018**, *4*, 501–515. [[CrossRef](#)]
165. Khamchiangta, D.; Dhakal, S. Time Series Analysis of Land Use and Land Cover Changes Related to Urban Heat Island Intensity: Case of Bangkok Metropolitan Area in Thailand. *J. Urban Manag.* **2020**, *9*, 383–395. [[CrossRef](#)]
166. Swain, D.; Roberts, G.J.; Dash, J.; Lekshmi, K.; Vinoj, V.; Tripathy, S. Impact of Rapid Urbanization on the City of Bhubaneswar, India. *Proc. Natl. Acad. Sci. India Sect. A Phys. Sci.* **2017**, *87*, 845–853. [[CrossRef](#)]
167. Wan, Z. New Refinements and Validation of the MODIS Land-Surface Temperature/Emissivity Products. *Remote Sens. Environ.* **2008**, *112*, 59–74. [[CrossRef](#)]
168. Fu, P.; Weng, Q. A Time Series Analysis of Urbanization Induced Land Use and Land Cover Change and Its Impact on Land Surface Temperature with Landsat Imagery. *Remote Sens. Environ.* **2016**, *175*, 205–214. [[CrossRef](#)]
169. Peres, L.D.F.; Lucena, A.J.D.; Rotunno Filho, O.C.; França, J.R.D.A. The Urban Heat Island in Rio de Janeiro, Brazil, in the Last 30 Years Using Remote Sensing Data. *Int. J. Appl. Earth Obs. Geoinf.* **2018**, *64*, 104–116. [[CrossRef](#)]
170. Athukorala, D.; Murayama, Y. Spatial Variation of Land Use/Cover Composition and Impact on Surface Urban Heat Island in a Tropical Sub-Saharan City of Accra, Ghana. *Sustainability* **2020**, *12*, 7953. [[CrossRef](#)]
171. Apolonio Callejas, I.J.; de Oliveira, A.S.; de Moura Santos, F.M.; Durante, L.C.; de Jesus Albuquerque Nogueira, M.C.; Zeilhofer, P. Relationship between Land Use/Cover and Surface Temperatures in the Urban Agglomeration of Cuiaba-Varzea Grande, Central Brazil. *J. Appl. Remote Sens.* **2011**, *5*, 053569. [[CrossRef](#)]
172. Silva, J.S.; da Silva, R.M.; Guimaraes Santos, C.A. Spatiotemporal Impact of Land Use/Land Cover Changes on Urban Heat Islands: A Case Study of Paco Do Lumiar, Brazil. *Build. Environ.* **2018**, *136*, 279–292. [[CrossRef](#)]
173. Imran, M.; Mehmood, A. Analysis and Mapping of Present and Future Drivers of Local Urban Climate Using Remote Sensing: A Case of Lahore, Pakistan. *Arab. J. Geosci.* **2020**, *13*, 278. [[CrossRef](#)]
174. Tucker, C.J. Red and Photographic Infrared Linear Combinations for Monitoring Vegetation. *Remote Sens. Environ.* **1979**, *8*, 127–150. [[CrossRef](#)]
175. Gillies, R.R.; Kustas, W.P.; Humes, K.S. A Verification of the “triangle” Method for Obtaining Surface Soil Water Content and Energy Fluxes from Remote Measurements of the Normalized Difference Vegetation Index (NDVI) and Surface e . *Int. J. Remote Sens.* **1997**, *18*, 3145–3166. [[CrossRef](#)]
176. Huete, A.R. A Soil-Adjusted Vegetation Index (SAVI). *Remote Sens. Environ.* **1988**, *25*, 295–309. [[CrossRef](#)]
177. Bannari, A.; Asalhi, H.; Teillet, P.M. Transformed Difference Vegetation Index (TDVI) for Vegetation Cover Mapping. In Proceedings of the IEEE International Geoscience and Remote Sensing Symposium, Toronto, ON, Canada, 24–28 June 2002; Volume 5, pp. 3053–3055.
178. Huete, A.; Didan, K.; Miura, T.; Rodriguez, E.P.; Gao, X.; Ferreira, L.G. Overview of the Radiometric and Biophysical Performance of the MODIS Vegetation Indices. *Remote Sens. Environ.* **2002**, *83*, 195–213. [[CrossRef](#)]

179. Zha, Y.; Gao, J.; Ni, S. Use of Normalized Difference Built-up Index in Automatically Mapping Urban Areas from TM Imagery. *Int. J. Remote Sens.* **2003**, *24*, 583–594. [[CrossRef](#)]
180. Xu, H. A New Index for Delineating Built-up Land Features in Satellite Imagery. *Int. J. Remote Sens.* **2008**, *29*, 4269–4276. [[CrossRef](#)]
181. As-syakur, A.R.; Adnyana, I.W.S.; Arthana, I.W.; Nuarsa, I.W. Enhanced Built-Up and Bareness Index (EBBI) for Mapping Built-Up and Bare Land in an Urban Area. *Remote Sens.* **2012**, *4*, 2957–2970. [[CrossRef](#)]
182. Xu, H. Analysis of Impervious Surface and Its Impact on Urban Heat Environment Using the Normalized Difference Impervious Surface Index (NDISI). *Photogramm. Eng. Remote Sens.* **2010**, *76*, 557–565. [[CrossRef](#)]
183. Rasul, A.; Balzter, H.; Ibrahim, G.R.F.; Hameed, H.M.; Wheeler, J.; Adamu, B.; Ibrahim, S.; Najmaddin, P.M. Applying Built-Up and Bare-Soil Indices from Landsat 8 to Cities in Dry Climates. *Land* **2018**, *7*, 81. [[CrossRef](#)]
184. Gao, B. NDWI—A Normalized Difference Water Index for Remote Sensing of Vegetation Liquid Water from Space. *Remote Sens. Environ.* **1996**, *58*, 257–266. [[CrossRef](#)]
185. McFeeters, S.K. The Use of the Normalized Difference Water Index (NDWI) in the Delineation of Open Water Features. *Int. J. Remote Sens.* **1996**, *17*, 1425–1432. [[CrossRef](#)]
186. Xu, H. Modification of Normalised Difference Water Index (NDWI) to Enhance Open Water Features in Remotely Sensed Imagery. *Int. J. Remote Sens.* **2006**, *27*, 3025–3033. [[CrossRef](#)]
187. Xiao, X.; Shen, Z.; Qin, X. Assessing the Potential of VEGETATION Sensor Data for Mapping Snow and Ice Cover: A Normalized Difference Snow and Ice Index. *Int. J. Remote Sens.* **2001**, *22*, 2479–2487. [[CrossRef](#)]
188. Zhao, H.; Chen, X. Use of Normalized Difference Bareness Index in Quickly Mapping Bare Areas from TM/ETM+. In Proceedings of the 2005 IEEE International Geoscience and Remote Sensing Symposium, 2005. IGARSS '05, Seoul, Korea, 29 July 2005; Volume 3, pp. 1666–1668.
189. McGarigal, K.; Cushman, S.A.; Neel, M.C.; Ene, E. *FRAGSTATS: Spatial Pattern Analysis Program for Categorical Maps*; The University of Massachusetts: Amherst, MA, USA, 2002.